High-pressure phase equilibrium and volumetric properties of pseudo-binary mixtures of stock tank oil + nitrogen/carbon dioxide up to 463K

Liu, Yiqun; Regueira, Teresa; Stenby, Erling H.; Yan, Wei

Published in:
Fluid Phase Equilibria

Link to article, DOI:
10.1016/j.fluid.2023.113929

Publication date:
2023

Document Version
Publisher's PDF, also known as Version of record

Fluid Phase Equilibria 576 (2024) 113929

Contents lists available at ScienceDirect

Fluid Phase Equilibria

journal homepage: www.journals.elsevier.com/fluid-phase-equilibria

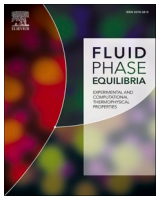

High-pressure phase equilibrium and volumetric properties of pseudo-binary mixtures of stock tank oil + nitrogen/carbon dioxide up to 463K

Yiqun Liu, Teresa Regueira, Erling H. Stenby, Wei Yan *

Center for Energy Resources Engineering (CERE), Department of Chemistry, Technical University of Denmark, Kgs. Lyngby DK-2800, Denmark

ARTICLE INFO

Keywords:
Density
Phase equilibrium
High-pressure
Reservoir fluid
Asymmetric systems

ABSTRACT

High-pressure phase equilibrium and volumetric properties are fundamental to developing high-pressure and high-temperature (HPHT) reservoirs. In this work, we extended our previous study on methane (CH_4) + stock tank oil (STO) to two other highly asymmetric light gas-STO systems: nitrogen (N_2) + STO and carbon dioxide (CO_2) + STO. We systematically measured their phase equilibrium and densities at temperatures from (298.15 to 463.15) K and pressures up to 140 MPa. The nitrogen mole fraction varies from 0.20 to 0.31 for the density measurement and from 0.21 to 0.40 for the phase equilibrium measurement. The carbon dioxide mole fraction varies from 0.20 to 0.70 for the density measurement and from 0.21 to 0.70 for the phase equilibrium measurement. We also determined the isothermal compressibilities and pseudo-excess volumes from the experimental densities. The measured data were modeled by the Soave-Redlich-Kwong (SRK) equation of state (EoS), the Peng-Robinson (PR) EoS, their volume translated versions SRK-VT and PR-VT, and the Perturbed Chain Statistical Associating Fluid Theory (PC-SAFT) EoS. For density, SRK and PR gave large deviations of ~16% and ~7%, respectively, compared with ~3% for PC-SAFT and PR-VT and ~1% for SRK-VT. The overall deviations for isothermal compressibility were in the range of 20~34% for all the models, with larger deviations for N_2+STO. SRK, PR, and PC-SAFT gave similar small deviations for pseudo-excess volumes. Using the excess volume method, these models could accurately estimate the live oil densities from the STO densities, showing an average deviation of ~0.5%. The deviations in predicted saturation pressures varied in a large range (4~16%), with PC-SAFT better for N_2+STO and SRK/PR better for CO_2+STO. The measured data and model comparison results are valuable for improving the phase behavior description for HPHT reservoir fluids and gas injection processes.

1. Introduction

In the oil industry, high-pressure high-temperature (HPHT) reservoirs [1,2] refer to those with a pressure higher than 69 MPa and a temperature higher than 150 °C. They are challenging and expensive to produce but can still be highly rewarding provided the reserve is large and the oil price is high. With the global transition towards sustainable energy, the use of fossil fuels will be gradually phased out. Nevertheless, the projected oil demand will stay high in the coming decades, and oil production from HPHT reservoirs or other challenging resources will still be relevant.

A major challenge for HPHT reservoirs is an accurate description of the phase equilibrium and thermophysical properties, not just at the original reservoir conditions but also at conditions for the entire production process. Therefore, HPHT also implies a larger temperature and pressure range to be covered. It should be noted that many reservoirs at quite high pressures may not satisfy the strict HPHT definition. However, they share a similar challenge in describing the equilibrium and thermophysical properties over a wide range. Apart from the wide temperature and pressure range, the challenge can be mainly attributed to the asymmetric nature of reservoir fluids, which are mixtures of hydrocarbons with large contrast in molecular size and property—non-hydrocarbons like nitrogen and carbon dioxide can play an important role and the term “hydrocarbon mixtures” is just a convenient simplification. Predicting the phase equilibrium in these highly asymmetric mixtures is generally difficult. It can be challenging even to describe their volumetric properties, like density and compressibility, over a wide temperature and pressure range.

In a broad sense, high-pressure phase equilibrium and

* Corresponding author.
E-mail address: weya@kemi.dtu.dk (W. Yan).

https://doi.org/10.1016/j.fluid.2023.113929
Received 10 June 2023; Received in revised form 8 August 2023; Accepted 14 August 2023
Available online 21 August 2023

Nomenclature

A_i	coefficients in Eq. (3)
B	constants in the Tammann-Tait equation Eq. (2)
B_i	coefficients in Eq. (2)
c	volume shift parameter for SRK or PR
C	constant in the Tammann-Tait equation Eq.(1)
k_{ij}	interaction parameter
MW	molecular weight
p	pressure
p_c	critical pressure
SG	specific gravity
T	temperature
T_c	critical temperature
v	molar volume
v_i^p	pure component molar volume for component i
V	volume
x_i	mole fraction
Z_{RA}	Rackett compressibility factor
ε	energy parameter
κ_T	isothermal compressibility
m	segment length
ρ	density
σ	segment diameter

Subscripts

0	reference properties for n-alkanes
PR	PR EoS
ref	reference
SRK	SRK EoS
STO	stock tank oil

Superscripts

E	excess properties
exp	experimental value
G	group
I	method I
II	method II
liq	liquid
cal	calculated value
sat	saturation point
tot	total
PE	pseudo-excess properties

Abbreviation

AARD	average absolute relative deviation
EoS	equation of state
G	gas
HPHT	high-pressure high-temperature
PC-SAFT	perturbed chain statistical associating fluid theory
PR	Peng-Robinson
SCN	single carbon number
SRK	Soave-Redlich-Kwong
STO	stock tank oil
TBP	true boiling point
VT	volume translation

thermophysical data for all the relevant binary, ternary, and multi-component mixtures [3–10] provide a basis for modeling HPHT reservoir fluids. However, experimental studies dedicated to HPHT fluids are more valuable but generally rare [9–19]. Our laboratory has recently carried out a series of such measurements [15–19] for well-defined mixtures and a real reservoir fluid. It was realized during these studies that the well-defined mixtures, in general, cannot represent reservoir fluids satisfactorily because the ill-defined C_{7+} fractions in the reservoir fluids can hardly be characterized by several physical components (although mathematically possible with artificial pseudo-components). Therefore, it is necessary to extend the experimental study to systems closer to the real reservoir fluids. We recently presented a study of CH_4 + stock tank oil (STO) [20], where the mixture equilibrium and volumetric properties at different compositions were measured and modeled. In this work, we extend our study to N_2+STO and CO_2+STO. The light gas-STO mixtures can be considered as pseudo-binary mixtures of two asymmetric components. They are not just a better analog to real reservoir fluids than the well-defined mixtures, but also sufficiently simple for investigating the interaction between light gases and STO. In addition, the study provides valuable knowledge to enhanced oil recovery through miscible or immiscible gas injection where CH_4, N_2, and CO_2 are widely used.

In the following sections, we first present the experimental and modeling methods. The same experimental and modeling methods are essentially used here as before [20]. Hence, we only provide a brief description while more details can be found in our previous study [20]. We then present the measurement and modeling results. Our measurement covers the temperature range from (298.15 to 463.15) K and pressures up to 140 MPa for both N_2+STO and CO_2+STO. The measured data are compared with the modeling results using two cubic equations of state (EoSs), Soave-Redlich-Kwong (SRK) [21] and Peng-Robinson (PR) [22], their volume translated (VT) versions SRK-VT and PR-VT, and a more advanced non-cubic EoS Perturbed Chain Statistical Associating Fluid Theory (PC-SAFT) [23]. The measurement and modeling results are discussed in comparison with those for CH_4+STO in our previous study.

2. Materials and methods

2.1. Materials

Nitrogen and carbon dioxide were purchased from AGA GAS A/B with a mole fraction purity of 99.999% and 99.995%, respectively. The stock tank oil (STO) sample was taken from a reservoir in the Danish sector of the North Sea. It was processed by centrifugation at 4000 rpm for 900 s to separate water. The STO composition was analyzed by true boiling point (TBP) distillation through a TBP distillation unit FISCHER technology Labodest HMS 500 AC. The determined composition up to the C_{24+} fraction and the molecular weight and density at 15.6 °C for each fraction were reported previously [20], and also presented in Table S1 in Supplementary Information. The standard uncertainty in the reported mole fractions is 0.002. The STO density at 288.75 K and 0.1 MPa is 0.8082 g·cm^{-3} while the C_7^+ density is 0.8151 g·cm^{-3}. The STO density was directly determined by a densimeter Anton Paar DMA 4100 while the density for C_7^+ fraction was calculated by removing the C_6 fraction from the measured STO densities. The molecular weight of the C_7^+ fraction is 197.39 g/mol. Prior to the experiment, the STO sample at ambient conditions is degassed for 3600s to remove any dissolved gas in oil by using an ultrasonic bath Branson 1510 DTH.

In our density and phase equilibrium measurements, we used pseudo-binary mixtures consisting of nitrogen or carbon dioxide as component 1 and STO as component 2. The STO is taken as one pseudo component here. The preparation procedure is slightly different for the density measurements and the phase equilibrium measurements since they used two different set-ups. For the density measurements, the pseudo-binary mixtures were prepared in an external high-pressure sample cylinder equipped with a floating piston, which separates the sample chamber and hydraulic fluid chamber. The STO was first added

Table 1
Composition[a] of the N_2/CO_2+STO mixtures for density and phase equilibrium measurement.

Pseudo binary mixture	Density	Phase Equilibrium
N_2 + STO		
	0.2016	0.2057
	0.3122	0.3086
		0.4044
CO_2 + STO	0.2028	0.2082
	0.4017	0.4000
	0.6044	0.6024
	0.7019	0.7013

[a] Standard mole fraction uncertainty $u(x)$: 0.002.

to the cylinder by using a burette (standard uncertainty 0.01 cm^3). Nitrogen or carbon dioxide stored in the small gas cylinder was then transferred to the cylinder, with the transferred mass measured accurately by an analytical balance Mettler-Toledo PR 1203 (standard uncertainty 0.001 g). The mixture of STO and gas was compressed to single-phase by a syringe pump (Teledyne ISCO 100 DX), which was connected to the hydraulic fluid side of the cylinder. The target pressure must be higher than the saturation pressure of the prepared mixture. The cylinder was rocked to ensure a homogeneous single-phase mixture. Table 1 lists the mole fraction of N_2 or CO_2 in the prepared mixtures. For the phase equilibrium measurements, the mixtures were prepared in the PVT cell directly. The STO was first added volumetrically to the PVT cell through a burette. The gas was transferred gravimetrically through an analytical digital balance to achieve a desired gas oil ratio. The compositions of the mixtures are presented in Table 1.

2.2. Density measurement

A schematic of the experimental setup for density measurement was previously reported [16]. The density was measured using a high-pressure vibrating tube density meter Anton Paar DMA HPM. The density meter measures the oscillation period of a U-tube filled with the sample fluid. The measured oscillating period had 7 significant digits with 3 digits after the decimal point. Our measurement covers the temperature range from (298.15 to 463.15) K and pressures up to 140 MPa. Temperature was controlled by a circulating bath Julabo PRESTO A30 and measured through a sensor Pt-100 located inside the measurement cell with a standard uncertainty of 0.02 K. Pressure was generated by a high-pressure generator HiP 37-6-30 and measured by a pressure transducer SIKA type P. This transducer could measure the pressure up to 150 MPa and its standard uncertainty of the full scale is 0.05 %. The expanded (k=2) uncertainty for the density measurement is 7×10^{-4} g/cm^3 at T<373.15K and 3×10^{-3} g/cm^3 at other temperatures.

Prior to the density measurement, the densimeter was calibrated following a modification of the method of Lagourette et al. [24] as previously reported [15,25]. Vacuum, Milli-Q water and n-dodecane with known densities were used as reference fluids for calibration. The density of n-decane was measured for validation. The measured values was compared with the literature data from Lemmon and Span [26] and Cibulka and Hnědkovský [27], giving a relative deviation of less than 0.3% [20].

2.3. Isothermal compressibility and pseudo-excess volume

The measured densities $\rho(T,p)$ are fitted to a modified Tammann-Tait equation: [28,29]

$$\rho(T,p) = \frac{\rho(T,p_{ref})}{1 - C\ln\left[\frac{B(T)+p}{B(T)+p_{ref}}\right]} \quad (1)$$

where p_{ref} refers to the reference pressure, C is a constant, $B(T)$ is a temperature dependent variable given by

$$B(T) = \sum_{j=0}^{2} B_j T^j \quad (2)$$

$\rho(T,p_{ref})$ is a polynomial of temperature:

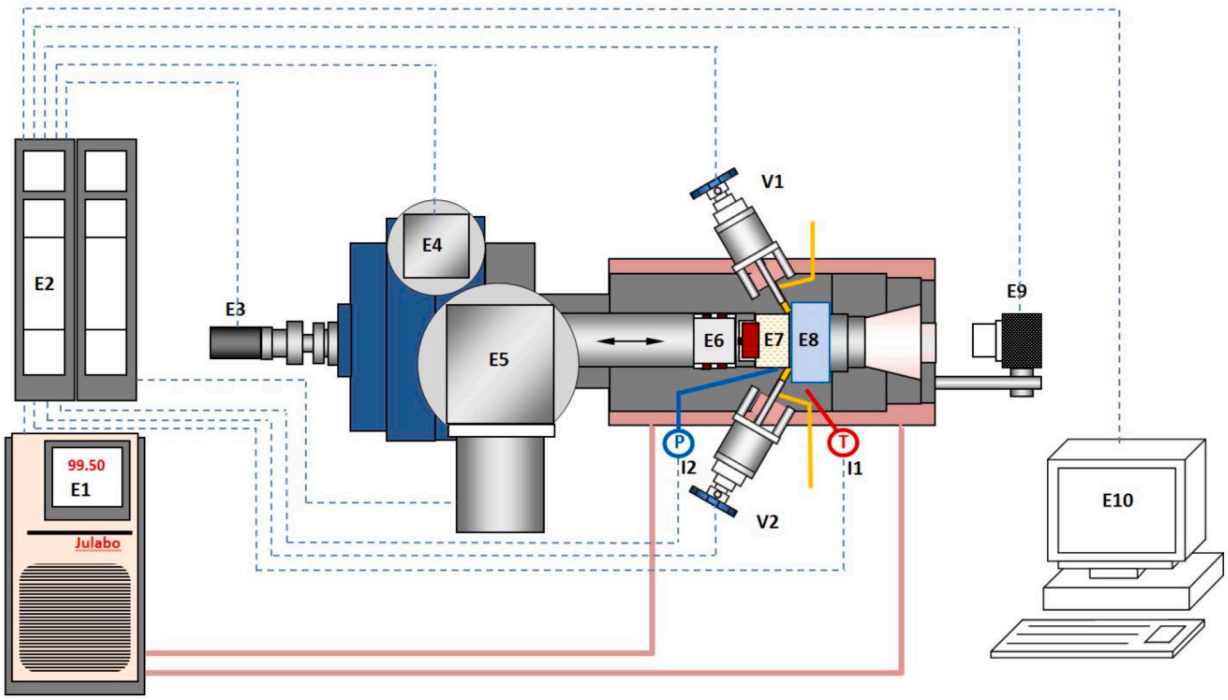

Fig. 1. Schematic of the PVT apparatus. (E1) thermostatic bath, (E2) control box, (E3) stirrer motor, (E4) piston motor, (E5) rotation system, (E6) piston with retractable blades, (E7) cell, (E8) sapphire window, (E9) video camera, (E10) computer, (I1) Pt100, (I2) pressure transducer, (V1, V2) high pressure valves.

Table 2
Experimental density values[a] (ρ) for the pseudo-binary system N_2 (1) + STO (2) in g·cm^{-3}.

	T/K					
p/MPa	298.15	323.15	348.15	373.15	423.15	463.15
	x_1=0.2016					
40	0.8069	0.7910	0.7743	0.7655	0.7330	0.7077
60	0.8181	0.8034	0.7879	0.7800	0.7505	0.7277
80	0.8286	0.8143	0.7998	0.7926	0.7651	0.7441
100	0.8380	0.8240	0.8103	0.8036	0.7778	0.7580
120	0.8465	0.8330	0.8198	0.8135	0.7889	0.7702
140	0.8546	0.8414	0.8286	0.8226	0.7990	0.7810
	x_1=0.3122					
60	0.8140	0.7989	0.7827	0.7744	0.7440	0.7202
80	0.8250	0.8108	0.7956	0.7880	0.7601	0.7381
100	0.8350	0.8215	0.8071	0.8001	0.7738	0.7533
120	0.8441	0.8309	0.8172	0.8107	0.7859	0.7665
140	0.8526	0.8398	0.8265	0.8202	0.7966	0.7782

[a] The expanded uncertainty for the density measurement $U(\rho)$ (k=2) is 7 × 10^{-4} g·cm^{-3} at T<373.15K and 3 × 10^{-3} g·cm^{-3} at other temperatures.

Table 3
Experimental density values[a] (ρ) for the CO_2 (1) + STO (2) system in g·cm^{-3}.

	T/K					
p/MPa	298.15	323.15	348.15	373.15	423.15	463.15
	x_1=0.2028					
10	0.8076	0.7885	0.7685	0.7497	0.7083	0.6737
20	0.8126	0.7946	0.7756	0.7604	0.7226	0.6918
40	0.8209	0.8047	0.7875	0.7781	0.7448	0.7186
60	0.8322	0.8170	0.8010	0.7926	0.7624	0.7389
80	0.8427	0.8280	0.8130	0.8053	0.7771	0.7552
100	0.8520	0.8378	0.8235	0.8164	0.7899	0.7695
120	0.8606	0.8468	0.8331	0.8264	0.8011	0.7817
140	0.8686	0.8552	0.8421	0.8356	0.8111	0.7927
	x_1=0.4017					
20	0.8216	0.8013	0.7800	0.7621	0.7186	0.6824
40	0.8317	0.8139	0.7947	0.7833	0.7462	0.7166
60	0.8445	0.8278	0.8102	0.8002	0.7670	0.7406
80	0.8561	0.8403	0.8237	0.8146	0.7838	0.7598
100	0.8664	0.8511	0.8355	0.8271	0.7983	0.7758
120	0.8759	0.8610	0.8461	0.8383	0.8109	0.7898
140	0.8846	0.8703	0.8560	0.8484	0.8221	0.8022
	x_1=0.6044					
20	0.8375	0.8121	0.7854	0.7616	–	–
40	0.8517	0.8297	0.8067	0.7913	0.7447	0.7077
60	0.8674	0.8473	0.8265	0.8132	0.7727	0.7413
80	0.8812	0.8624	0.8431	0.8313	0.7944	0.7662
100	0.8934	0.8754	0.8575	0.8467	0.8125	0.7864
120	0.9044	0.8872	0.8701	0.8600	0.8279	0.8034
140	0.9146	0.8980	0.8817	0.8721	0.8414	0.8183
	x_1=0.7019					
20	0.8499	0.8189	0.7861	–	–	–
40	0.8684	0.8421	0.8150	0.7953	0.7398	0.6957
60	0.8869	0.8633	0.8392	0.8227	0.7756	0.7391
80	0.9030	0.8810	0.8588	0.8443	0.8021	0.7698
100	0.9169	0.8960	0.8755	0.8623	0.8235	0.7939
120	0.9294	0.9095	0.8900	0.8778	0.8416	0.8140
140	0.9408	0.9217	0.9032	0.8917	0.8573	0.8311

[a] The expanded uncertainty for the density measurement $U(\rho)$ (k=2) is 7 × 10^{-4} g·cm^{-3} at T<373.15K and 3 × 10^{-3} g·cm^{-3} at other temperatures.

$$\rho(T, p_{ref}) = \sum_{i=0}^{3} A_i T^i \tag{3}$$

The isothermal compressibility (κ_T) is calculated by

$$\kappa_T(T,p) = \frac{1}{\rho}\left(\frac{\partial \rho}{\partial p}\right)_T \tag{4}$$

The relative expanded isothermal compressibility uncertainty $U_r(\kappa_T)$ (k=2) is 0.02.

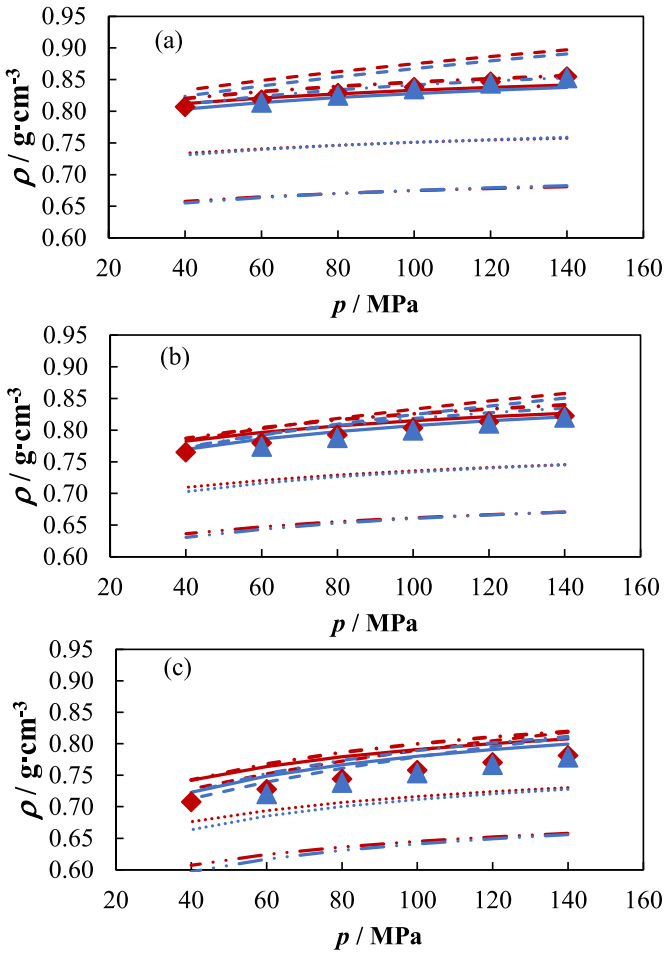

Fig. 2. Density of the N_2 (1) + STO (2) system at (a) 298.15 K, (b) 373.15 K and (c) 463.15 K. Points represent experimental measurement: (◆) x_1=0.2016 and (▲) x_1=0.3122. Lines represent model predictions: (— • •) SRK, (•••) PR, (– –) PC-SAFT, (– •) SRK-VT, and (—) PR-VT.

We define the pseudo-excess volume (v^{PE})for the pseudo-binary mixture of STO and gas as follows:

$$v^{PE} = v - (x_G v_G + x_{STO} v_{STO}) \tag{5}$$

where x_G and x_{STO} are the mole fractions of the gas and the STO, respectively, and v_G and v_{STO} are the molar volumes of the gas and the STO, respectively. The molar volumes v_G for nitrogen and carbon dioxide in this study are taken from the NIST database while the STO molar volumes v_{STO} are directly calculated from the measured STO densities.

2.4. Phase equilibrium measurement

The phase equilibrium measurement was carried out in the PVT 240/1500 FV apparatus from Sanchez Technologies. A schematic of this experimental setup is presented in Fig. 1, as previously reported in [17]. The PVT cell is a variable volume cell. A motor driven piston is used to change the system volume. The piston is equipped with retractable blades at its head to stir the sample. There is a sapphire window at the cell bottom to realize full visibility. Phase change is monitored through the window by a CCD digital camera. The liquid fraction can also be measured by locating the boundary between two phases. The cell is heated by a set of heating resistances located in the wall of the cell along with a thermostating liquid circulating in a jacket around the cell. The temperature is measured through a Pt-100 with a standard uncertainty of 0.02 K. The pressure in the cell is measured through a transducer

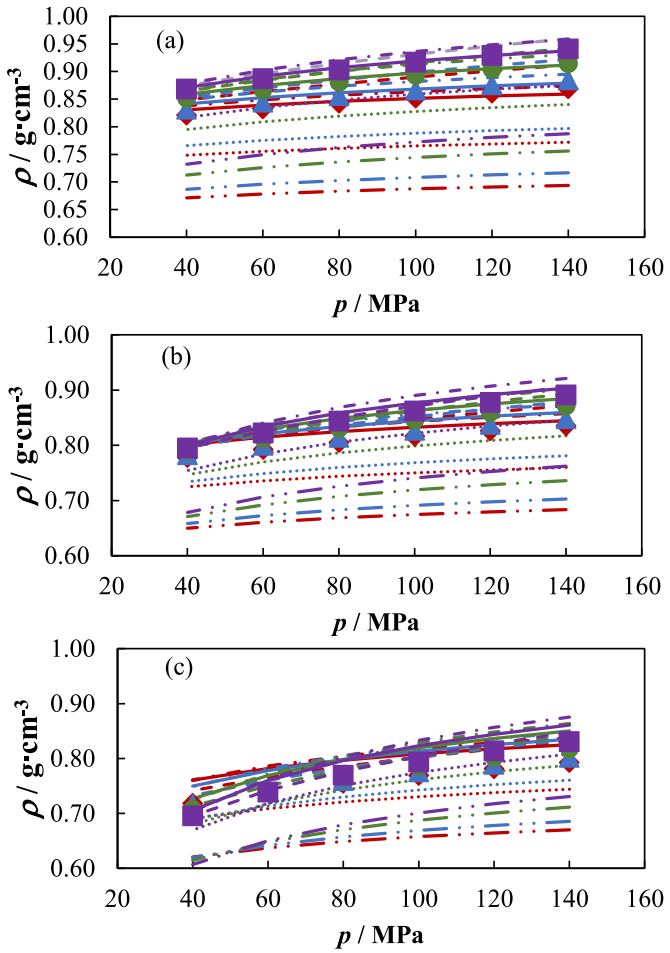

Fig. 3. Density of the CO_2 (1) + STO (2) system at (a) 298.15 K, (b) 373.15 K and (c) 463.15 K. Points represent experimental data: (◆) x_1=0.2028, (▲) x_1=0.4017, and (●) x_1=0.6044 and (■) x_1=0.7019. Lines represent model predictions: (— • •) SRK, (•••) PR, (– –) PC-SAFT, (– •) SRK-VT and (—) PR-VT.

Dynisco PT435A with a standard deviation of 0.06 MPa. The system is fully controlled by means of the Falcon software.

The apparatus was used to measure the saturation pressure (always bubble point pressure in this study), the liquid fraction in the two-phase region. The measurement was carried out in a constant mass expansion (CME) procedure, which involves stepwise pressure decrease for the same fluid mixture. The change in the slope of the pressure-volume curve can be used to roughly locate the bubble point. Nevertheless, the accurate bubble point pressure was determined by decreasing the pressure from single-phase region with a flow rate of 5.6×10^{-4} $cm^3 \cdot s^{-1}$ until the appearance of a bubble/cloud was observed through visual observation. This measurement was performed in triplicate. The combined standard uncertainty of the saturation pressure measurement is estimated to be 0.1 MPa. The uncertainty is considered to be satisfactory for reservoir fluid related PVT study. To determine the liquid fraction in the two-phase region, the system was stirred for 300 s and then stabilized for 600 s until the pressure became stable within 0.05 MPa. The (*p, V, T*) conditions in the cell were then recorded with a photo taken of the fluid inside. The photo was subsequently analyzed using the Euclide software for the liquid fraction V^{liq}/V^{tot} where V^{liq} is the liquid volume and V^{tot} is the total volume of the system at the measurement conditions. In addition, the relative volume can be readily calculated from its definition V^{tot}/V^{sat} where V^{sat} is the volume of the system at the saturation point. The maximum standard liquid fraction uncertainty u (liquid fraction percentage) is estimated to be 2.1 %. The liquid fraction data is not as important as the bubble pressure data since the modeling

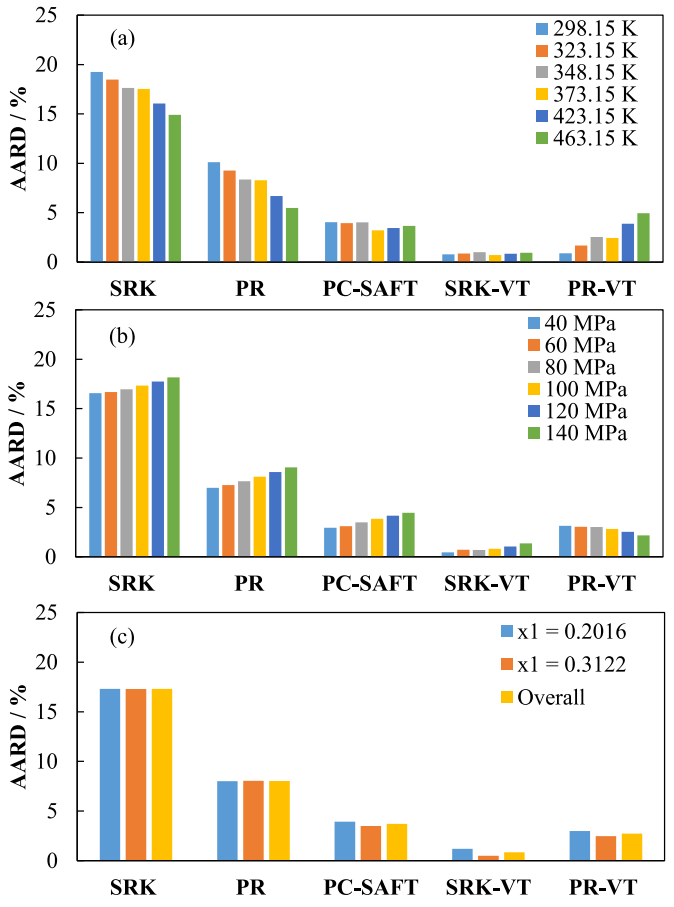

Fig. 4. AARD (%) in the density prediction for the N_2 (1) + STO (2) system by different models: (a) as a function of temperature, (b) as a function of pressure, and (c) as a function of composition and overall deviation.

of liquid fraction is affected by the deviations in both phase equilibrium and density and an exact matching of the liquid fraction is usually not required.

2.5. Data modeling

We chose two classical cubic equations of state (EoSs), Soave-Redlich-Kwong (SRK) [21] and Peng-Robinson (PR) [22], and one non-cubic EoS, PC-SAFT [23], to model the measured systems. For the modeling of volumetric properties (density, isothermal compressibility, and excess volume), the volume translated versions for SRK and PR were also used.

2.5.1. SRK, PR and their volume-translated versions

We used SRK and PR with the classical van der Waals one-fluid mixing rules. Regarding the model parameters, we need the critical temperatures T_{ci}, critical pressures p_{ci}, and acentric parameters ω_i for pure components, and a binary interaction parameter k_{ij}between two components i and j. We adopted the k_{ij}values regressed in a previous study [30]. The Peneloux volume translation [31] is used to improve the density calculation by SRK and PR. The resulting models are denoted by SRK-VT and PR-VT, respectively. The molar volumes for the original SRK and PR, v_{SRK} and v_{PR}, are corrected by

$$v_{SRK-VT} = v_{SRK} - c_{SRK} \tag{6}$$

$$v_{PR-VT} = v_{PR} - c_{PR} \tag{7}$$

where v_{SRK-VT} and v_{PR-VT} are the molar volumes after the volume

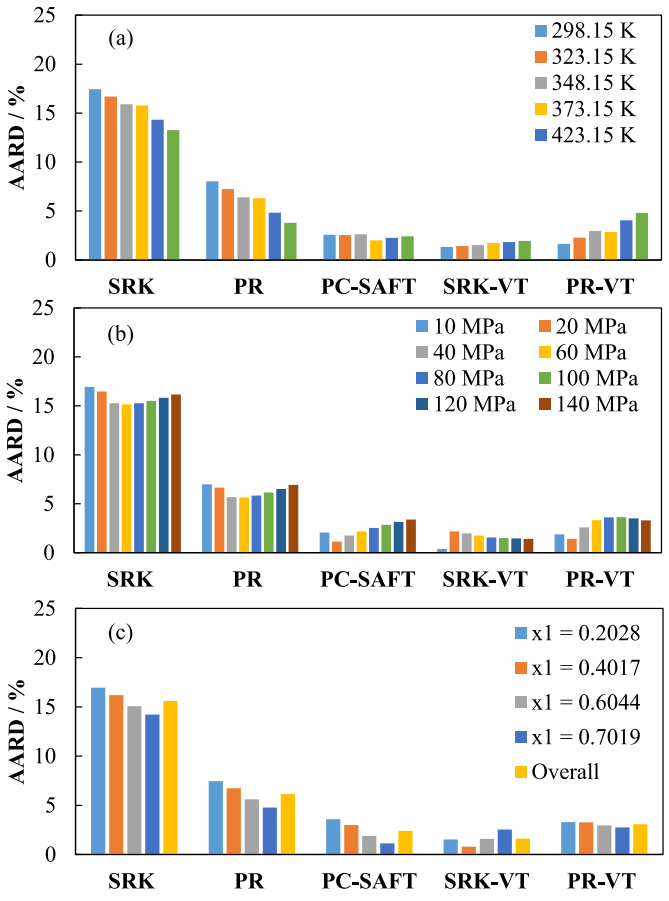

Fig. 5. AARD (%) in the density prediction of the CO_2 (1) + STO (2) system by different models: (a) as a function of temperature, (b) as a function of pressure, and (c) as a function of composition and overall deviation.

Table 4
Fitting parameters of the modified Tammann-Tait equation and AARD (%) for the density of the N_2 (1) + STO (2) system.

	x_1=0.2016	x_1=0.3122
p_{ref} / MPa	40	60
A_0 /g·cm^{-3}	0.4580	1.3493
$10^3 A_1$ /g·cm^{-3}·K^{-1}	4.0606	-3.6228
·K-1		
·A1 /g·cm-3		
·K-1		
$10^6 A_2$ /g·cm^{-3}·K^{-2}	-13.7556	8.3632
·K-2		
·A2 /g·cm-3		
·K-2		
$10^9 A_3$ /g·cm^{-3}·K^{-3}	13.1111	-7.5051
C	0.0950	0.0982
B_0 /MPa	314.5079	249.2032
·K-1		
·A1 /g·cm-3		
·K-1		
B_1 / MPa·K^{-1}	-1.0632	-0.7007
·K-2		
·A2 /g·cm-3		
·K-2		
$10^4 B_2$ / MPa·K^{-2}	8.5761	3.9799
·K-3		
·A3 /g·cm-3		
·K-3		
AARD/%	0.38	0.13

Table 5
Fitting parameters of the modified Tammann-Tait equation and AARD (%) for the density of the CO_2 (1) + STO (2) system.

	x_1=0.2028	x_1=0.4017	x_1=0.6044	x_1=0.7019
p_{ref} / MPa	10	20	40	20
A_0 /g·cm^{-3}	1.2402	1.3395	1.3864	1.9646
$10^3 A_1$ /g·cm^{-3}·K^{-1}	-2.6130	-3.2817	-3.21704	-8.1119
·K-1				
·A1 /g·cm-3				
·K-1				
$10^6 A_2$ /g·cm^{-3}·K^{-2}	5.4459	7.2032	6.6034	20.8716
·K-2				
·A2 /g·cm-3				
·K-2				
$10^9 A_3$ /g·cm^{-3}·K^{-3}	-5.2756	-6.8677	-6.0930	-20.9202
C	0.0948	0.0961	0.1024	0.0933
B_0 /MPa	456.2727	366.1848	360.9155	282.2657
·K-1				
·A1 /g·cm-3				
·K-1				
B_1 / MPa·K^{-1}	-1.6040	-1.2584	-1.3342	-1.1017
·K-2				
·A2 /g·cm-3				
·K-2				
$10^4 B_2$ / MPa·K^{-2}	14.4576	10.6612	11.8169	10.0181
·K-3				
·A3 /g·cm-3				
·K-3				
AARD/%	0.16	0.14	0.14	0.14

Table 6
Isothermal compressibility[a] ($10^3 \cdot \kappa_T$) for the N_2 (1) + STO (2) system in MPa^{-1}.

	T/K					
p/MPa	298.15	323.15	348.15	373.15	423.15	463.15
	x_1=0.2016					
40	0.76	0.83	0.94	1.08	1.23	1.63
60	0.66	0.72	0.80	0.89	1.00	1.25
80	0.59	0.64	0.70	0.77	0.84	1.02
100	0.53	0.57	0.62	0.67	0.73	0.86
120	0.49	0.52	0.56	0.60	0.65	0.75
140	0.45	0.47	0.51	0.54	0.58	0.66
	x_1=0.3122					
60	0.72	0.79	0.86	0.95	1.17	1.40
80	0.64	0.69	0.75	0.81	0.96	1.12
100	0.57	0.61	0.66	0.71	0.82	0.93
120	0.52	0.55	0.59	0.63	0.72	0.80
140	0.48	0.51	0.54	0.57	0.64	0.71

[a] The relative expanded isothermal compressibility uncertainty $Ur(\kappa_T)$ (k=2) is 0.02.

translation for SRK and PR, respectively; c_{SRK} and c_{PR} are the volume translation parameters for SRK and PR, respectively. For a mixture, c_{SRK} and c_{PR} must be calculated using a linear mixing rule

$$c = \sum_i x_i c_i \tag{8}$$

where c is the volume translation parameter (c_{SRK} or c_{PR}) for the mixture and c_i is the parameter for pure component i ($c_{SRK,i}$ or $c_{PR,i}$). We used the following correlations [32] for well-defined components lighter than C_7:

$$c_{SRK,i} = 0.40768 \frac{RT_{ci}}{P_{ci}} \left(0.29441 - Z_{RA,i}\right) \tag{9}$$

$$c_{PR,i} = 0.50033 \frac{RT_{ci}}{P_{ci}} \left(0.25969 - Z_{RA,i}\right) \tag{10}$$

Here, $Z_{RA,i}$ is the Rackett compressibility factor [33] expressed by:

$$Z_{RA,i} = 0.29056 - 0.08775\omega_i \tag{11}$$

Table 7
Isothermal compressibility[a] ($10^3 \cdot \kappa_T$) for the CO_2 (1) + STO (2) system in MPa^{-1}.

	T/K					
p/MPa	298.15	323.15	348.15	373.15	423.15	463.15
	x_1=0.2028					
10	0.81	0.96	1.14	1.37	2.04	2.83
20	0.75	0.88	1.03	1.21	1.71	2.23
40	0.66	0.75	0.86	0.99	1.30	1.59
60	0.59	0.66	0.75	0.84	1.06	1.24
80	0.53	0.59	0.66	0.73	0.89	1.03
100	0.49	0.53	0.59	0.65	0.77	0.88
120	0.45	0.49	0.53	0.58	0.68	0.77
140	0.41	0.45	0.49	0.53	0.62	0.68
	x_1=0.4017					
20	0.91	1.06	1.24	1.48	2.15	3.00
40	0.78	0.88	1.01	1.16	1.54	1.94
60	0.68	0.76	0.85	0.96	1.21	1.45
80	0.61	0.67	0.74	0.82	1.00	1.16
100	0.55	0.60	0.66	0.72	0.86	0.97
120	0.50	0.54	0.59	0.64	0.75	0.84
140	0.46	0.50	0.54	0.58	0.67	0.74
	x_1=0.6044					
40	0.95	1.10	1.29	1.52	2.14	2.81
60	0.81	0.92	1.05	1.20	1.56	1.90
80	0.71	0.80	0.89	1.00	1.24	1.45
100	0.64	0.70	0.78	0.86	1.04	1.18
120	0.58	0.63	0.69	0.75	0.89	1.00
140	0.53	0.57	0.62	0.67	0.78	0.87
	x_1=0.7019					
40	1.16	1.36	1.61	1.93	2.85	3.97
60	0.95	1.09	1.24	1.43	1.91	2.42
80	0.81	0.91	1.02	1.15	1.45	1.77
100	0.71	0.78	0.87	0.96	1.18	1.41
120	0.63	0.69	0.75	0.83	0.99	1.17
140	0.57	0.62	0.67	0.73	0.86	1.01

[a] The relative expanded isothermal compressibility uncertainty $Ur(\kappa_T)$ (k=2) is 0.02.

2.5.2. PC-SAFT

For the PC-SAFT EoS [23], we used its simplified version proposed by von Solms et al. [34] Compared with the original PC-SAFT, the simplified PC-SAFT (sPC-SAFT) provides exactly the same results for pure components and almost equal results for mixtures. It means that the pure component parameters for sPC-SAFT and PC-SAFT are exchangeable. The main advantage of sPC-SAFT over the original PC-SAFT is its speed, especially for associating compounds. In this study, we denote the simplified version by PC-SAFT for simplicity.

For non-associating components studied here, each pure component has three model parameters, including the segment length, the segment diameter, and the energy parameter. For mixtures, there is an interaction parameter k_{ij} for each *i*-*j* pair. The three pure component parameters are taken from [23] and the k_{ij} taken from [30].

2.5.3. C_{7+} characterization

To model ill-defined petroleum fluid, it is necessary to characterize its ill-defined C_{7+} fraction. For SRK and PR, we adopted the method of Pedersen et al. [35,36] but used a different set of correlations for the critical parameters T_{ci}, P_{ci}, and ω_i. Specifically, we chose Twu's correlations [37] for T_{ci} and P_{ci}, and the Lee-Kesler correlations [39,40] for ω_i. The single carbon number (SCN) components above C_7 were lumped into 12 pseudo-components with nearly equal mass. For PC-SAFT, we adopted the method of Yan et al. [30] The method is similar to the method of Pedersen et al. [35,36] The major difference lies in the estimation of the model parameters for the SCN components—The PC-SAFT parameters m, ε, and $\sigma$are estimated in the method of Yan et al. [30] The estimation is through a two-step perturbation approach. For a SCN component with boiling point T_b and specific gravity SG, we first estimate the parameters of the n-alkane at this T_b. The n-alkane molecular weight, MW_0, can be estimated using Twu's correlations. [37] The

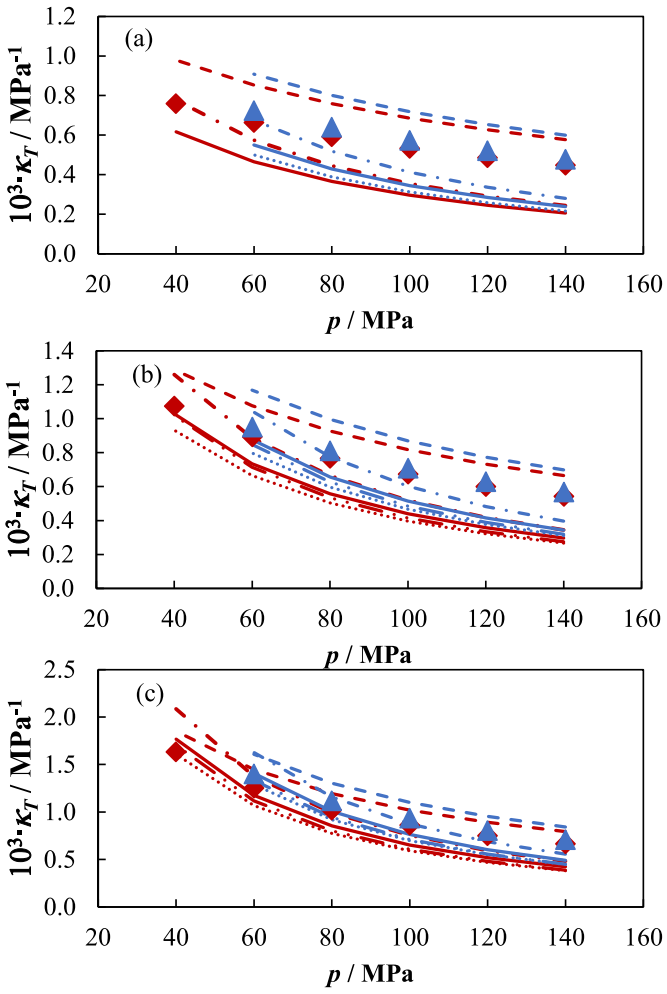

Fig. 6. Isothermal compressibility (κ_T) of the N_2 (1) + STO (2) system at (a) 298.15 K, (b) 373.15 K, and (c) 463.15 K. Points represent experimental data: (◆) x_1=0.2016 and (▲) x_1=0.3122. Lines represent model predictions: (— • •) SRK, (•••) PR, (– –) PC-SAFT, (– •) SRK-VT, and (—) PR-VT.

PC-SAFT parameters for the n-alkane, m_0, ε_0 and σ_0, are calculated through simple linear correlations [30]:

$$m_0 = 0.02644MW_0 + 0.83500 \tag{12}$$

$$m_0\varepsilon_0/k = 6.90845MW_0 + 139.30870 \tag{13}$$

$$m_0\sigma_0^3 = 1.71638MW_0 + 19.19189 \tag{14}$$

In the second step, we estimate the parameters of the SCN component using the difference in specific gravity $SG - SG_0$ as a perturbation parameter, where SG_0 is the specific gravity of the n-alkane calculated by Soave's correlation. [38] The PC-SAFT parameters for the SCN component are estimated by [30]

$$\sigma = \sigma_0 \tag{15}$$

$$\varepsilon = \varepsilon_0(1.1303391\Delta SG + 1) \tag{16}$$

$$m = m_0\left(1.0460471\Delta SG^2 - 1.6209973\Delta SG + 1\right) \tag{17}$$

The model parameters for the pure and lumped components, including the pure component parameters and the k_{ij}, are provided in Tables S2 to S5 in Supplementary Information. It should be noted that the C_7^+ volume translation parameters for SRK and PR were generated by matching the STO density at atmospheric pressure. In this sense, the characterization for SRK-VT and PR-VT has included some experimental

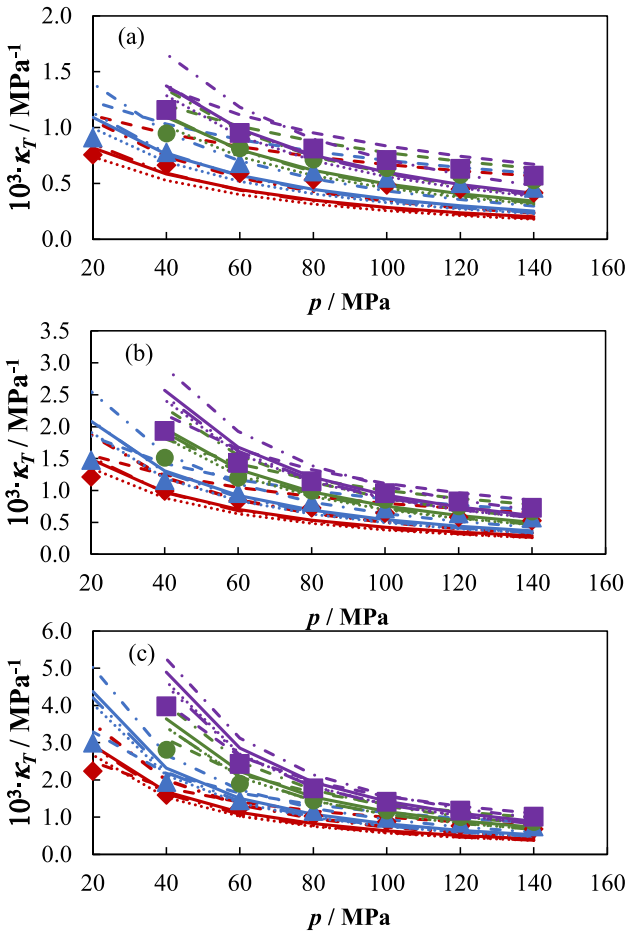

Fig. 7. Isothermal compressibility (κ_T) of the CO_2 (1) + STO (2) system at (a) 298.15 K, (b) 373.15 K, and (c) 463.15 K. Points represent experimental data: (◆) x_1=0.2028, (▲) x_1=0.4017, (●) x_1=0.6044, and (■) x_1=0.7019. Lines represent model predictions: (— • •) SRK, (•••) PR, (– –) PC-SAFT, (– •) SRK-VT, and (—) PR-VT.

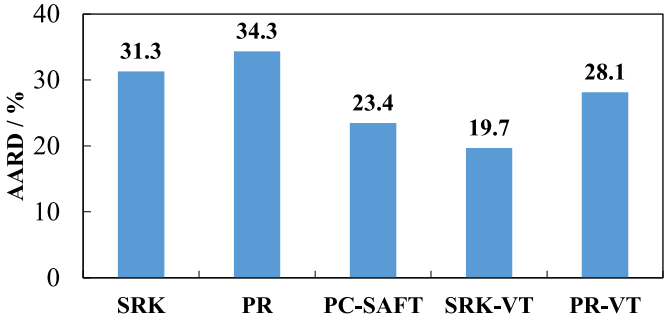

Fig. 8. AARD (%) in the isothermal compressibility (κ_T) prediction for the N_2 (1) + STO (2) system by different models.

density information, which is not included in that for PC-SAFT.

3. Results and discussion

We present experimental data for density, isothermal compressibility, pseudo-excess molar volume, saturation pressure, liquid fraction, and relative volume along with their modeling results. In most comparisons, we use the average absolute relative deviation (AARD) defined by

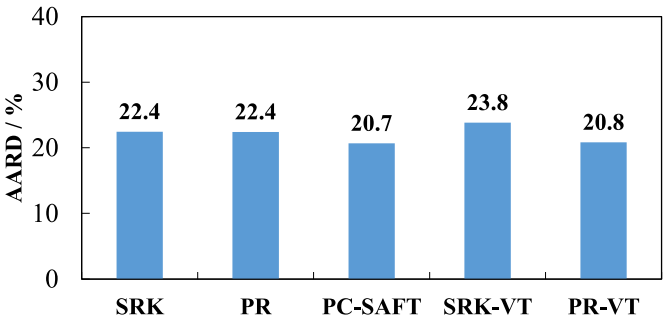

Fig. 9. AARD (%) in the isothermal compressibility (κ_T) prediction for the CO_2 (1) + STO (2) system by different models.

Table 8
Pseudo-excess volume (v^{PE}) for the N_2 (1) + STO (2) system in $cm^3 \cdot mol^{-1}$.

	T/K					
p/MPa	298.15	323.15	348.15	373.15	423.15	463.15
x_1=0.2016						
40	-6.25	-7.11	-7.80	-8.58	-9.77	-10.61
60	-3.35	-3.90	-4.24	-4.66	-5.29	-5.73
80	-2.12	-2.46	-2.67	-2.92	-3.31	-3.57
100	-1.45	-1.66	-1.81	-1.98	-2.18	-2.47
120	-0.99	-1.18	-1.27	-1.40	-1.53	-1.75
140	-0.73	-0.88	-0.92	-1.02	-1.12	-1.25
x_1=0.3122						
60	-5.81	-6.64	-7.22	-7.98	-9.12	-9.86
80	-3.84	-4.47	-4.80	-5.29	-6.11	-6.53
100	-2.80	-3.32	-3.54	-3.90	-4.40	-4.83
120	-2.13	-2.55	-2.71	-3.01	-3.44	-3.74
140	-1.71	-2.06	-2.15	-2.38	-2.76	-3.02

$$AARD\,/\% = \frac{100}{k}\sum_{i=1}^{k}\left|\frac{Y^{cal} - Y^{exp}}{Y^{exp}}\right| \tag{18}$$

where Y is the value of the analyzed property and k is the number of experimental data points, The superscripts *cal* and *exp* represent the calculated and experimental, respectively. In the comparison for the pseudo-excess molar volume (v^{PE}), we use a different deviation AARD*:

$$AARD^{*}\,/\% = \frac{100}{k}\sum_{i=1}^{k}\left|\frac{v^{PE,cal} - v^{PE,exp}}{v^{exp}}\right| \tag{19}$$

where v^{PE} is the pseudo-excess molar volume and v is the molar volume. The experimental molar volume is used as the scaling parameter so that AARD* can reflect how the absolute deviation in v^{PE} will affect the molar volume or density calculation.

3.1. Density

Tables 2 and 3 present the measured high-pressure densities for N_2+STO and CO_2+STO, respectively. Both systems cover six temperatures from (298.15 to 463.15) K and pressures up to 140 MPa. However, only two compositions were measured for N_2+STO while four compositions for CO_2+STO. This is because the bubble point pressure in N_2+STO becomes very high even at x_1=0.3122. Our previous study of CH_4+STO [20] has the same six temperatures and the same upper pressure limit, but three compositions up to x_1=0.6133. Since CO_2 has a much higher solubility in STO, we could reach a higher x_1=0.7019 in CO_2+STO.

The density modeling results are presented in Figs. 2 and 3. Only three temperatures are selected to give an overview of the trends in density and the performance of different models. The density increases

Table 9
Pseudo-excess volume (v^{PE}) for the CO_2 (1) + STO (2) system in $cm^3 \cdot mol^{-1}$.

	T/K					
p/MPa	298.15	323.15	348.15	373.15	423.15	463.15
x_1=0.2028						
10	-0.18	-11.82	-25.92	-34.00	-45.63	-52.61
20	0.71	-0.33	-2.39	-5.88	-12.73	-16.69
40	1.19	0.87	0.56	-0.01	-1.53	-2.86
60	1.33	1.13	1.05	0.84	0.31	-0.19
80	1.34	1.21	1.21	1.12	0.88	0.72
100	1.36	1.25	1.27	1.23	1.18	0.97
120	1.35	1.26	1.29	1.28	1.27	1.16
140	1.32	1.23	1.27	1.29	1.34	1.25
x_1=0.4017						
20	0.30	-1.80	-6.10	-13.22	-26.93	-34.85
40	1.29	0.59	-0.20	-1.51	-4.80	-7.63
60	1.57	1.16	0.84	0.24	-1.10	-2.24
80	1.65	1.37	1.22	0.88	0.15	-0.41
100	1.68	1.47	1.39	1.15	0.75	0.33
120	1.69	1.53	1.47	1.29	1.03	0.74
140	1.69	1.53	1.50	1.37	1.19	0.96
x_1=0.6044						
20	-0.28	-3.26	-9.62	-20.11	–	–
40	1.09	0.20	-1.00	-2.96	-7.50	-11.39
60	1.47	0.99	0.46	-0.45	-2.24	-3.92
80	1.63	1.29	0.99	0.42	-0.52	-1.42
100	1.67	1.44	1.23	0.80	0.25	-0.36
120	1.69	1.49	1.36	1.04	0.65	0.23
140	1.67	1.51	1.41	1.14	0.88	0.58
x_1=0.7019						
20	-0.64	-3.81	-10.85	–	–	–
40	0.81	-0.06	-1.31	-3.42	-8.18	-12.16
60	1.18	0.74	0.21	-0.77	-2.60	-4.31
80	1.30	1.03	0.75	0.13	-0.83	-1.74
100	1.35	1.17	0.98	0.53	-0.05	-0.65
120	1.35	1.22	1.10	0.74	0.34	-0.06
140	1.33	1.23	1.14	0.85	0.57	0.29

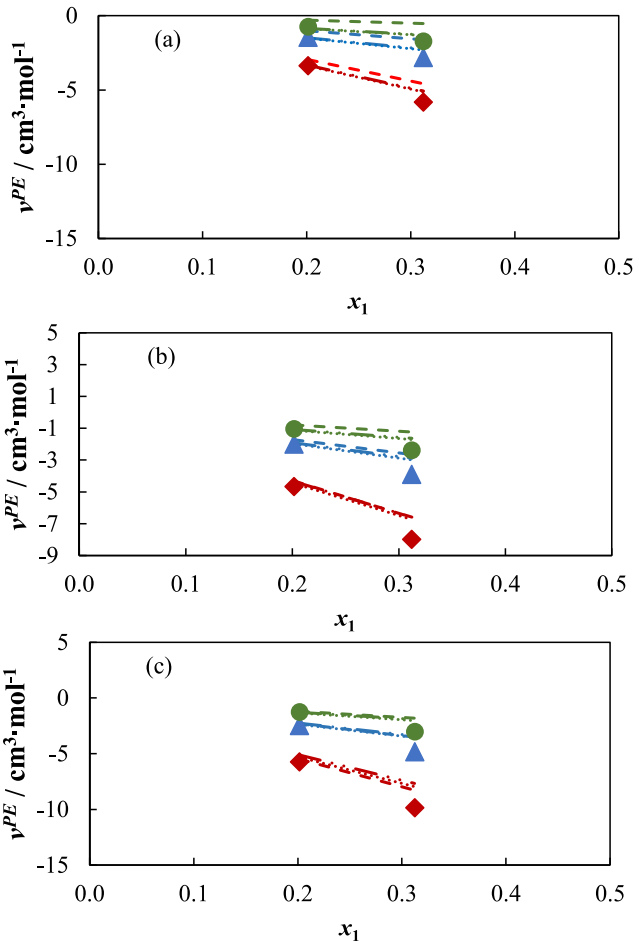

Fig. 10. Pseudo-excess volume (v^{PE}) of the N_2 (1) + STO (2) system at (a) 298.15 K, (b) 373.15 K and (c) 463.15 K. Points represent experimental measurement: (◆) 60 MPa, (▲) 100 MPa, and (●) 140 MPa. Lines represent model predictions through (— • •) SRK, (•••) PR and (– –) PC-SAFT.

with pressure and decreases with temperature, with the temperature effect more pronounced than the pressure one for the studied ranges. The composition influence is more complicated. For N_2+STO, the density decreases with the gas mole fraction, which is similar to the trend for CH_4+STO [20]. For CO_2+STO, there is a clear density increase with the CO_2 mole fraction, a trend just the opposite to that for N_2+STO and CH_4+STO. The opposite trends can be attributed to the difference in the mass densities of CO_2, CH_4 and N_2. For example, the mass densities for these three components at 323.15 K and 40 MPa are 0.9233, 0.2262, and 0.3344 $g \cdot cm^{-3}$, respectively. The much higher CO_2 density is caused by its larger molar mass and smaller molar volume. Since CO_2 has a much higher T_c than CH_4 and N_2, it is at a more compressed liquid-like state with a much smaller molar volume (its compressibility factor is 0.7096, as compared to 1.0559 for CH_4 and 1.2473 for N_2). It is worthwhile to note that the high density is somewhat related to the T_c and p_c of CO_2. If we compare CO_2 with propane (C_3H_8) that has a very similar molar mass, the mass density of C_3H_8 at the same condition is only 0.5362 $g \cdot cm^{-3}$. The main reason for the large density contrast is that CO_2 has a much smaller T_c/P_c ratio than C_3H_8, thus giving a smaller co-volume or a smaller molar volume at a compressed state (propane's compressibility factor is 1.2243). In fact, CO_2 shows a higher mass density than the STO in many of the studied conditions. The density increase with increasing CO_2 mole fraction can largely be explained by the high mass density of CO_2, although other factors, like the excess molar volume, also plays a role, especially at lower pressures.

All the models can readily capture the correct pressure trends and, in general, the temperature and composition trends. It should be noted that SRK and PR predict intersecting isotherms at two adjacent compositions in Fig. 2. The measured data do not indicate such a trend. However, the trends predicted by SRK-VT and PR-VT are correct. The modeling deviations are better illustrated in Figs. 4 and 5. It is not surprising that SRK and PR without volume translation give the worst predictions (SRK being the poorest). Once volume translation is applied, with the volume shift parameters determined by fitting the C_{7+} density, the deviations are reduced by many times to a level comparable to that from PC-SAFT. We previously observed a similar effect of volume translation for CH_4+STO [20]. Actually, SRK-VT shows the smallest overall deviation for both systems. PR-VT is similar to PC-SAFT, giving a slightly lower deviation for N_2+STO and a slightly larger deviation for CO_2+STO. In comparison, PR-VT gives the smallest deviation for CH_4+STO [20]. In addition, it is possible to find some correlations between the deviation with temperature, pressure, or composition in Figs. 4 and 5. For instance, PC-SAFT tends to perform worse at a higher pressure and PR-VT seems poorer at a higher temperature. It was also observed for CH_4+STO that PC-SAFT gives a larger deviation at a higher pressure. Nevertheless, these observations are limited to the studied systems and conditions and should not be generalized. It is worth mentioning that deviation in Figs. 4 and 5 show certain similarity to that for STO [20] in terms of its temperature and pressure dependence and the relative magnitudes for different models. This also indicates the close relation between the STO density modeling and the mixture density modeling, which was observed for CH_4+STO [20]. Therefore, if we want to capture the live fluid density accurately over a large pressure and temperature range, it is crucial to model the STO density accurately over the same range.

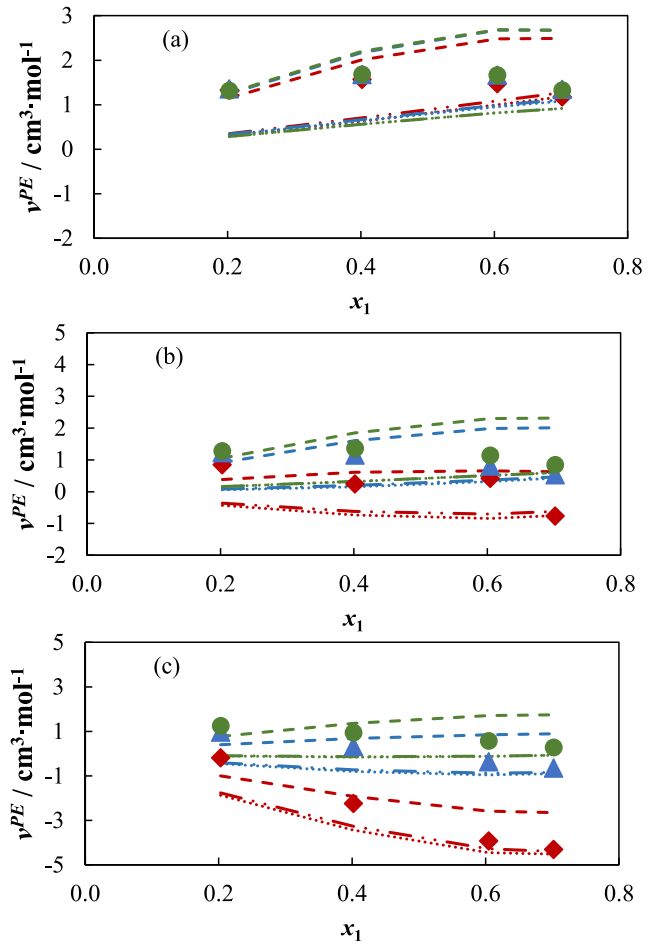

Fig. 11. Pseudo-excess volume (v^{PE}) of the CO_2 (1) + STO (2) system at (a) 298.15 K, (b) 373.15 K, and (c) 463.15 K. Points represent experimental data: (◆) 60 MPa, (▲) 100 MPa and (●) 140 MPa. Lines represent model predictions through (— • •) SRK, (•••) PR and (– –) PC-SAFT.

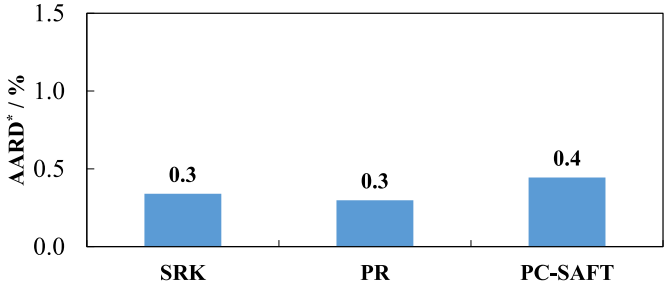

Fig. 12. AARD* (%) in the predicted pseudo-excess volume of the N_2 (1) + STO (2) system by different models.

3.2. Isothermal compressibility

Tables 4 and 5 provide the parameters in a modified Tammann-Tait equation (Eq. (1)) obtained by fitting the mixture data at different compositions for N_2+STO and CO_2+STO, respectively. The corresponding fitting deviations are also provided. The isothermal compressibility data were generated using Eq. (4), i.e., by differentiating the modified Tammann-Tait equation. Tables 6 and 7 present the calculated isothermal compressibility data. The data, together with the modeling results, at three selected temperatures are shown in Fig. 6 for N_2+STO and Fig. 7 for CO_2+STO. In general, a higher pressure, a lower temperature, or a lower amount of dissolved gas results in a lower

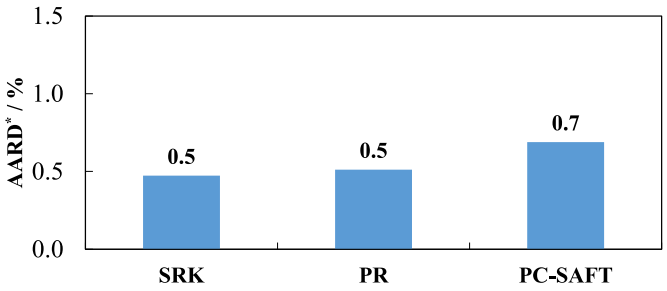

Fig. 13. AARD* (%) in the predicted pseudo-excess volume of the CO_2 (1)+ STO (2) system by different models.

compressibility. At the same temperature, pressure, and gas mole fraction, the compressibilities for CO_2+STO, N_2+STO, and CH_4+STO are similar, with those for CO_2+STO being slightly higher at low pressures. The calculated compressibility from different models generally follows the trend in Figs. 6 and 7, but the relative deviations are large. Figs. 8 and 9 summarize the deviations in compressibility (more details on the deviations at different composition in Figs. S1 and S2 in Supplementary Information). All models perform similarly, with SRK-VT and PR-VT giving better results than SRK and PR for N_2-STO but comparable results for CO_2-STO. PC-SAFT is similar to SRK-VT and PR-VT. Our previous study [20] showed that SRK and PR are clearly much worse than the other three models for STO but only slightly poorer for CH_4-STO. Actually, the deviations by PC-SAFT, SRK-VT, and PR-VT are around 20% for all three systems, as compared to around 3% for STO. The deviations by SRK and PR are around 32%, 25%, and 22% for N_2-STO, CH_4-STO, and CO_2-STO, respectively, as compared to 18% (SRK) and 8.5% (PR) for STO. The above deviations show that for "heavy" liquid without dissolved gas or at a higher reduced pressure or lower reduced temperature, models with better density results have a clear advantage in compressibility modeling. With the addition of gas, their advantage becomes less pronounced. Since the solubility magnitude is N_2<CH_4<CO_2, the deviation decreases from 32% to 22%. At a higher gas mole fraction, SRK and PR still give poor densities, but the isothermal compressibility becomes closer due to cancellation of errors. Figs. S1 and S2 in Supplementary Information provide more detailed deviations at different gas fractions. For CO_2-STO, there is a trend that the compressibility deviation becomes smaller at higher mole fractions.

3.3. Pseudo-excess volume

The molar pseudo-excess volume v^{PE} is a concept based on the pseudo binary mixture assumption, i.e., a live oil can be considered as a mixture of STO and stock tank gas (STG). The treatment of any live oil as a mixture of STO and STG is known as the black oil model in reservoir engineering. STG can be a gas mixture although our study so far only involves pure gases like CH_4, N_2, and CO_2. It should be noted that v^{PE} is not equal to the molar excess volume v^E unless both STO and STG are ideal mixtures at the temperature and pressure of interest, or their combination happens to be ideal mixing due to cancellation of errors. Nevertheless, v^{PE} has important practical applications despite the subtle difference between v^{PE} and v^E. In this subsection, we first present v^{PE} calculated by Eq. (5) for both N_2+ STO and CO_2+ STO, and then show how to estimate the live oil density using the excess molar volume method.

Tables 8 and 9 present the experimental v^{PE} for N_2+STO and CO_2+STO, respectively. Figs. 10 and 11 illustrate the experimental v^{PE} at three selected temperatures and three selected pressures, together with the modeling results from SRK, PR, and PC-SAFT. Since the volume translation does not change excess volume and its influence on pseudo-excess volume is negligible, we exclude SRK-VT and PR-VT in the discussion.

For N_2+STO, v^{PE} is negative in the studied range. It becomes more

Table 10
Overall deviations for calculated densities using different methods[a].

N_2 + STO					
	SRK	PR	PC-SAFT	SRK-VT	PR-VT
Original models	17.30 (20.31)	8.03 (11.36)	3.72 (5.01)	2.73 (5.66)	1.73 (4.96)
Excess volume method I	**0.25** (1.00)	0.46 (0.70)	**0.23** (0.51)	**0.21** (0.86)	**0.24** (0.85)
Excess volume method II	0.34 (1.13)	**0.30** (0.99)	0.44 (0.82)	-	-
CO_2 + STO					
	SRK	PR	PC-SAFT	SRK-VT	PR-VT
Original models	15.61 (20.11)	6.14 (11.13)	2.40 (5.02)	3.07 (6.44)	2.07 (5.83)
Excess volume method I	0.84 (4.73)	1.29 (2.62)	0.75 (1.81)	1.02 (2.79)	0.73 (2.11)
Excess volume method II	**0.48** (1.29)	**0.51** (1.50)	**0.68** (1.74)	-	-

[a] The deviations are the mean values of AARD (%) and the numbers in the parentheses are the maximum values.

negative with increasing temperature and less negative with increasing pressure. Although only two compositions were measured, it can still be seen that v^{PE} decreases with the N_2 mole fraction. A v^{PE} minimum can be expected at a higher mole fraction if the system does not split into two phases at that condition. The above trends for N_2+STO are very similar to those for CH_4+STO while the v^{PE} for N_2+STO is generally more negative under the same conditions.

For CO_2+STO, v^{PE} generally decreases with temperature and

Table 11
Saturation pressure[a] (p^{sat}) for the pseudo-binary system N_2 (1) + STO (2).

x_1=0.2057		x_1=0.3086		x_1=0.4044	
T/K	p^{sat}/MPa	T/K	p^{sat}/MPa	T/K	p^{sat}/MPa
298.16	23.19	298.12	40.66	298.15	–
323.14	21.93	323.12	38.53	323.14	68.73
348.22	20.28	348.15	35.71	348.23	58.14
373.23	18.79	373.24	32.93	373.16	50.59
423.15	16.42	423.12	27.66	423.15	40.96
463.09	14.85	463.13	24.38	463.21	35.04

[a] Standard temperature uncertainty $u(T)$: 0.02 K; Combined standard pressure uncertainty $u(p)$:0.10 MPa.

Table 12
Saturation pressure[a] (p^{sat}) for the pseudo-binary system CO_2 (1) + STO (2).

x_1=0.2082		x_1=0.4000		x_1=0.6024		x_1=0.7013	
T/K	p^{sat}/MPa	T/K	p^{sat}/MPa	T/K	p^{sat}/MPa	T/K	p^{sat}/MPa
298.16	1.93	298.15	3.92	298.19	5.79	298.17	6.47
323.09	2.47	323.19	5.15	323.17	8.27	323.18	9.71
348.18	3.03	348.17	6.44	348.21	10.87	348.16	13.52
373.18	3.57	373.16	7.74	373.21	13.33	373.18	16.56
423.19	4.70	423.20	9.90	423.15	17.18	423.20	21.00
463.17	5.45	463.21	11.24	463.16	19.16	463.18	22.21

[a] Standard temperature uncertainty $u(T)$: 0.02 K; Combined standard pressure uncertainty $u(p)$:0.10 MPa.

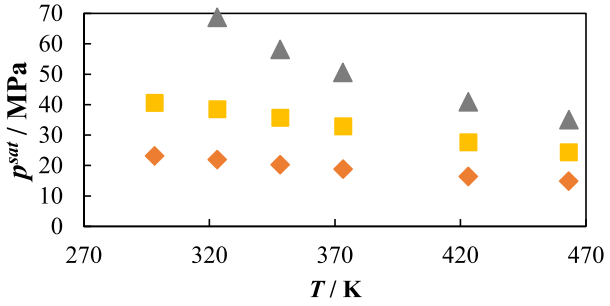

Fig. 14. Saturation pressure (p^{sat}) of the N_2 (1) + STO (2) system at (◆) x_1=0.2057, (■) x_1=0.3086, (▲) x_1=0.4044.

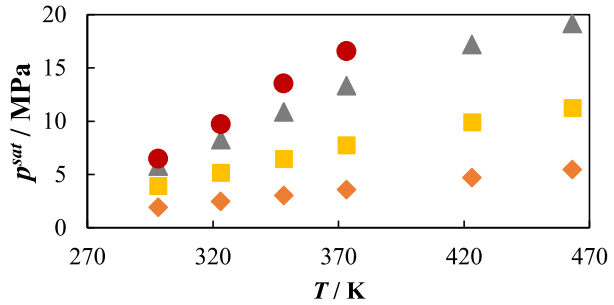

Fig. 15. Saturation pressure (p^{sat}) of the CO_2 (1) + STO (2) system at (◆) x_1=0.2082, (■) x_1=0.4000, (▲) x_1=0.6024, and (●) x_1=0.7013.

increases with pressure. Many of the measured values are positive at lower temperatures and higher pressures, which is a distinctive feature in comparison with N_2+STO and CH_4+STO. In addition, v^{PE} does not always decrease with the CO_2 mole fraction although the general trend is still decreasing.

All three models give close predictions for N_2+STO. SRK and PR are very similar and PC-SAFT shows a larger difference from the other two at 298.15 K and 140 MPa. For CH_4+STO, PC-SAFT also shows some difference from the other two models [20]. The modeling deviations for CO_2+STO are larger, and none of the models can exactly capture the trend with composition. PC-SAFT again shows different results from the other two. Figs. 12 and 13 present the scaled deviations for v^{PE} calculated using Eq. (12), which reflect how the absolute deviation in v^{PE} will affect the fluid density. For N_2+STO, they are lower than 0.5%. Even for CO_2+STO where the absolute deviations seem larger, the scaled deviations are barely above 0.5%. Three models only show slight difference and PC-SAFT is not as good as SRK and PR.

The low scaled deviations indicate that in the density modeling, the major deviations are from the deviations in the STO and gas densities. If we obtain accurate densities for the STO and gas (N_2 or CO_2), we can use v^{PE} calculated by a model to estimate the mixture density with good accuracy. This excess volume method [8] was discussed in our recent study of high-pressure densities, where we showed that different cubic- and non-cubic models gave similar excess volumes. The excess volume method can be applied to other thermodynamic properties, but it is only used to calculate density here. The method consists in evaluating the mixture molar volume using two different models:

$$v = \sum x_i v_i^{p,II} + v^{E,I} \tag{20}$$

The pure-component molar volumes v_i^p are obtained from model II, which can be understood as a more accurate source for pure component densities. The molar excess volumes $v^{E,I}$ are obtained from an EoS model I, which can be a simpler model or an easily accessible model. For reservoir fluids, we use the pseudo-excess volume instead:

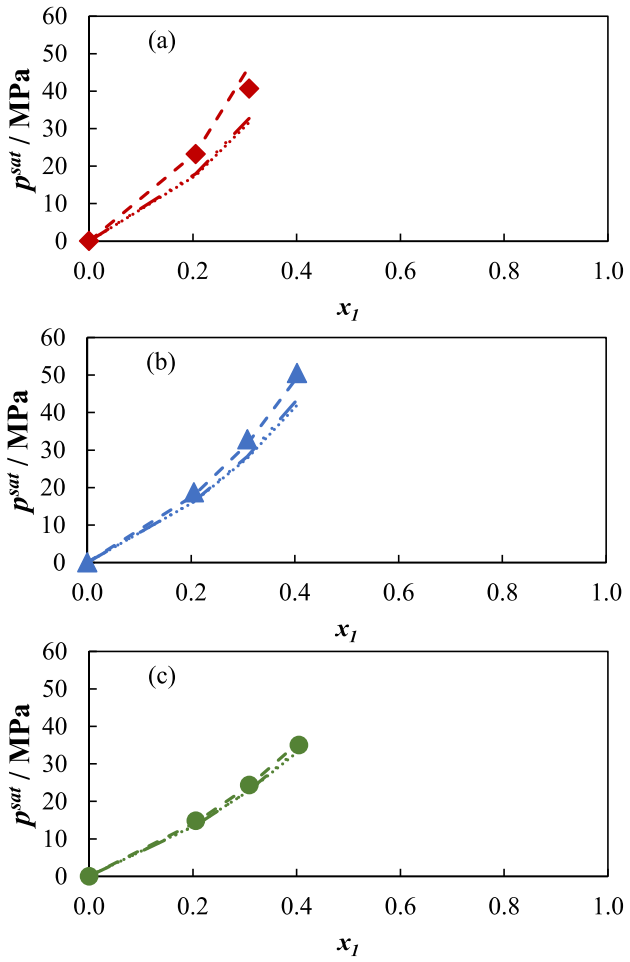

Fig. 16. Saturation pressure (p^{sat}) of the N_2(1) + STO (2) system at (a) 298.15 K, (b) 373.15 K and (c) 463.15 K. Lines represent model predictions: (— • •) SRK, (•••) PR, and (– –) PC-SAFT.

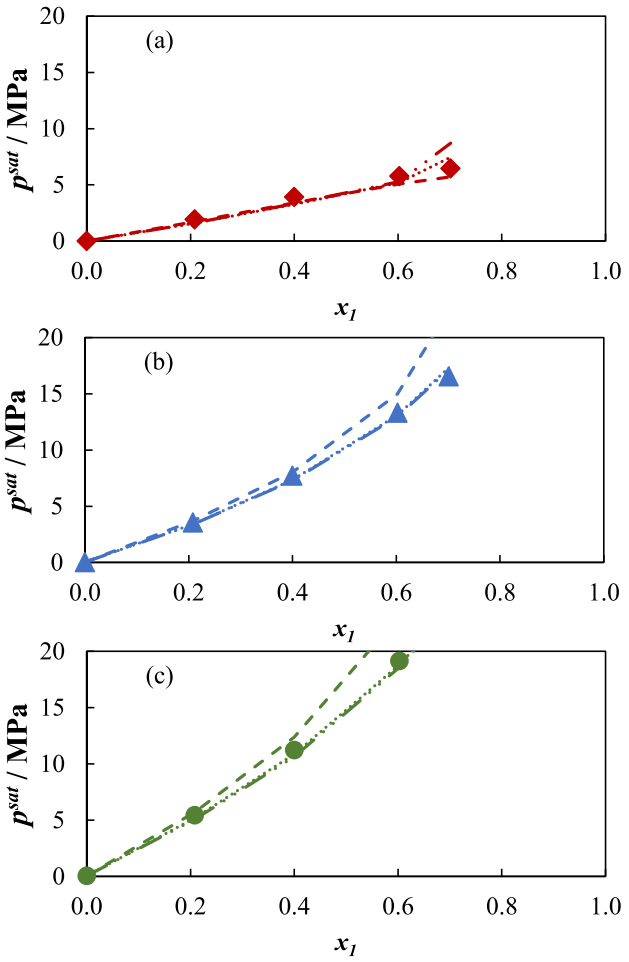

Fig. 17. Saturation pressure (p^{sat}) of the CO_2 (1) + STO (2) system at (a) 298.15 K, (b) 373.15 K, and (c) 463.15 K. Lines represent model predictions: (— • •) SRK, (•••) PR, and (– –) PC-SAFT.

$$v = \sum x_i v_i^p + x_{STO} v_{STO} + v^{PE} \tag{21}$$

where STO is treated as one pseudo-component with its mole fraction x_{STO} and its molar volume v_{STO}, and the remaining components are treated as individual components with their mole fractions $x_i$and pure component molar volumes v_i^p. Since there is only one gas component, the summation term can be simplified to $x_G v_G$, where x_G is the gas mole fraction and v_G is the pure gas molar volume. To test the excess volume method, we combine the v^{PE} calculated by different models with the v_{STO} from the experimental STO densities and the v_G calculated in the following two ways:

- Excess volume method I: $v_G$calculated by the same model used for v^{PE}.
- Excess volume method II: v_G from NIST

Table 10 summarizes the overall deviations for both N_2+STO and CO_2+STO systems using the two excess volume methods. We provide both the mean value of AARD and the maximum of AARD (in parentheses). The volume translation does not have any effect in the second method. Therefore, we only include SRK-VT and PR-VT in the first method. It is obvious that the excess volume method can significantly reduce both the mean and maximum deviations even compared with PC-SAFT, SRK-VT, and PR-VT. We marked in bold the smallest mean deviation for each model. The smallest deviations for different models are comparable, showing that the result is insensitive to the model for v^{PE}.

The smallest mean deviations are around 0.25% for N_2+STO and 0.5% for CO_2+STO, as compared to 1% for CH_4+STO [20]. The extremely small deviations for N_2+STO are partly due to its narrower composition range. For N_2+STO, the two methods are similar with the first method being slightly better. Actually, the first method gives a more accurate N_2 density, but the cancellation of errors may give a larger effect at this low deviation level. For CO_2+STO, the advantage of using more accurate CO_2 density is clear, with the second method giving much lower deviations. The results further confirm the effectiveness of the excess volume method in density modeling. The method can also be used to provide accurate density estimation with a minimum experimental effort.

3.4. Saturation pressure

Tables 11 and 12 present the saturation pressures (p^{sat}) measured for N_2+STO at three compositions and for CO_2+STO at four compositions in the temperature range from (298 to 463) K. The measured saturation pressures, also shown in Figs. 14 and 15, constitute three partial phase envelopes for each system. The influence of temperature on the saturation pressure can be clearly seen in the two figures. The saturation pressure for N_2+STO always decreases with temperature whereas that for CO_2+STO always increases with temperature. In comparison, CH_4+STO shows a decreasing trend at its highest CH_4 concentration (x_1=0.8063), an increasing trend at its two lowest concentrations (x_1=0.2046 and 0.4039), and a transition behavior at the intermediate concentrations [20]. For a typical multicomponent reservoir fluid

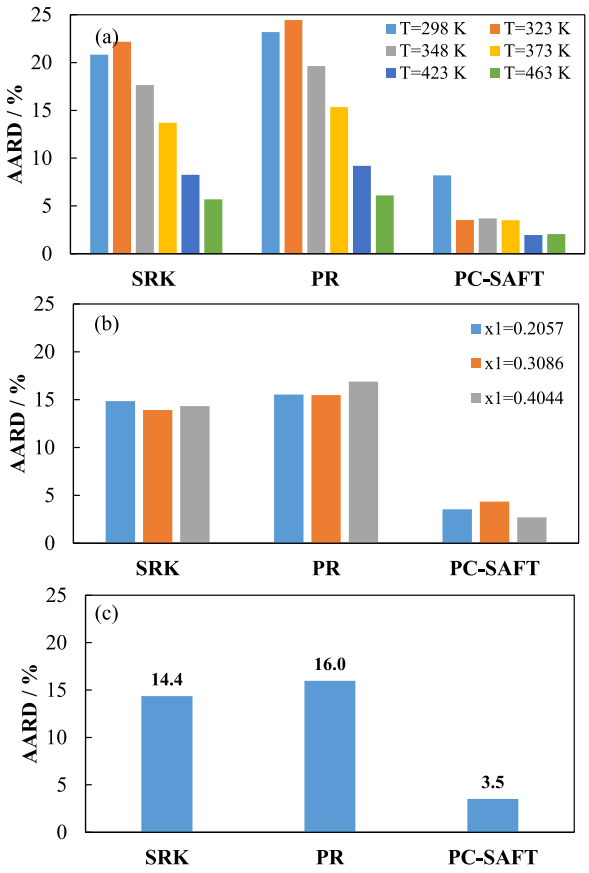

Fig. 18. AARD (%) in predicted saturation pressure for the N_2 (1) + STO (2) system by different models: (a) as a function of temperature, (b) as a function of N_2 mole fraction (x_1), and (c) overall deviation.

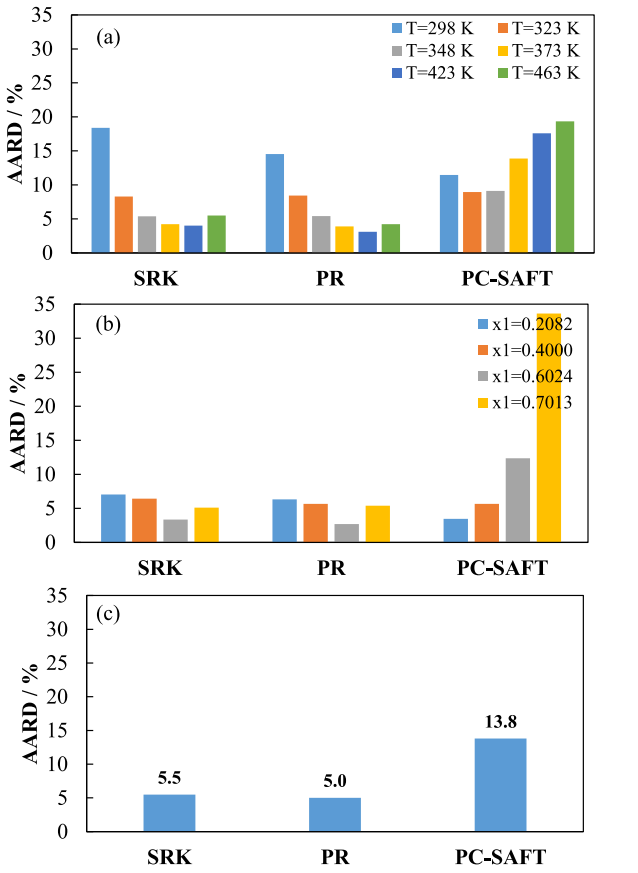

Fig. 19. AARD (%)in the saturation pressure of the CO_2 (1) + STO (2) system by different models (a) as a function of temperature, (b) as a function of CO_2 mole fraction (x_1), and (c) overall deviation.

mixture, its bubble point pressure usually increases with temperature when the condition is far from the critical point but decreases with temperature when the condition is closer to the critical point (provided that the critical point is in the decreasing segment of the envelope). In other words, a heavier mixture, like black oil, tends to give an increasing trend whereas a lighter mixture, like volatile oil, tends to give a decreasing trend. For the three gas components, their solubilities in STO follow the order: CO_2>CH_4>N_2. At the same gas mole fraction, the mixture with N_2 appears to be a lighter mixture and that with CO_2 appears to be a heavier one. That is why we observed an increasing trend in p^{sat} for CO_2, a decreasing trend for N_2, and a transitional behavior for CH_4 (decreasing at higher gas fractions and increasing at lower ones). Nevertheless, the quantitative behavior must be determined experimentally.

The saturation pressure always increases with the gas mole fraction in the studied range, as shown in Figs. 16 and 17 for N_2+STO and CO_2+STO, respectively, and for CH_4+STO in our previous study. It should be noted that such an increasing trend is valid only for the composition range investigated since a decreasing trend may be observed for the saturation pressure, usually dew point pressures, at high concentrations. However, such a transition from a bubble point to a dew point is not easy to measure in pure gas + STO systems because it is difficult to dissolve all the heavy components in STO in the absence of intermediate components. A large two-phase region may form at higher concentrations instead, which is clearer for N_2+STO. In general, the solubility in STO shows an order N_2<CH_4<CO_2, corresponding to the opposite order in the saturation pressure at the same gas mole fraction: N_2>CH_4>CO_2.

Figs. 16 and 17 also show the modeling results by SRK, PR, and PC-SAFT. For N_2+STO, PC-SAFT gives the best description whereas SRK and PR tend to underpredict the saturation pressure, particularly at low temperatures. Fig. 18 summarizes the AARD% for the three models. PC-SAFT gives a deviation smaller than 5% as compared with around 15% for SRK and PR. All the models tend to give lower deviations at higher temperatures. For CO_2+STO, SRK and PR give a much better description than PC-SAFT, and PC-SAFT tends to overshoot. As shown in Fig. 19, PC-SAFT gives a deviation around 14% as compared with around 5% for SRK and PR, and it clearly shows a high deviation at the highest composition. It is worth mentioning that PC-SAFT performs slightly better for CH_4+ STO [20] and much better for several well-defined systems [15–19]. Obviously, the performance of these models in phase equilibrium calculation is case-dependent and there is no clear superiority of one model over another. It also underscores the importance of phase equilibrium measurement.

3.5. *Relative volume and liquid fraction*

The relative volume (V^{tot}/V^{sat}) and the liquid fraction (V^{liq}/V^{tot}) in the two-phase region are two properties typically measured in a reservoir fluid PVT study. They are useful for regressing the PVT model, and the liquid fraction is important for the phase behavior description in the two-phase region. However, they are not as important as the saturation pressure. In the model evaluation using the two properties, it should be noted that the relative volume and liquid fraction in the two-phase region depend on the both the two-phase equilibrium modeling and the density modeling, making it difficult to assign the deviation to a single source.

Tables 13 and 14 presents the measured data of these two properties for N_2+STO and CO_2+STO, respectively. In Supplementary Information, we plot the properties at three selected temperatures along with the

Table 13
Relative volume (V^{tot}/V^{sat}) and liquid fraction (V^{liq}/V^{tot}) for the pseudo-binary system N_2 (1) + STO (2)[a].

x_1=0.2057								
298 K			373 K			463 K		
p/MPa	V^{tot}/V^{sat}	V^{liq}/V^{tot}	p/MPa	V^{tot}/V^{sat}	V^{liq}/V^{tot}	p/MPa	V^{tot}/V^{sat}	V^{liq}/V^{tot}
32.87	0.986		29.07	0.983		30.37	0.957	
30.89	0.99		26.81	0.986		25.45	0.971	
29.25	0.991		24.91	0.989		23.16	0.977	
27.25	0.992		22.94	0.991		21.17	0.982	
25.39	0.993		20.93	0.994		19.14	0.988	
24.42	0.996		19.09	0.997		17.02	0.994	
24.00	0.997		19.04	0.998		15.06	0.999	
23.19	1	1	18.79	1	1	14.85	1	1
21.92	1.005	–	18.08	1.006	–	14.80	1.002	–
19.10	1.018	–	16.61	1.019	0.988	14.49	1.007	–
15.19	1.045	0.972	14.27	1.046	0.973	13.84	1.023	–
10.83	1.104	0.931	11.19	1.102	0.934	12.61	1.045	–
6.40	1.256	0.834	7.35	1.245	0.833	10.75	1.096	0.934
3.59	1.568	0.685	4.44	1.535	0.692	7.96	1.226	0.836
1.94	2.194	0.519	2.55	2.118	0.514	5.37	1.489	0.701
1.15	3.135	0.376	1.61	2.994	0.390	3.41	2.016	0.521
0.75	4.39		1.11	4.164		2.33	2.809	0.386
						1.71	3.866	
x_1=0.3086								
298 K			373 K			463 K		
p/MPa	V^{tot}/V^{sat}	V^{liq}/V^{tot}	p/MPa	V^{tot}/V^{sat}	V^{liq}/V^{tot}	p/MPa	V^{tot}/V^{sat}	V^{liq}/V^{tot}
45.85	0.988		43.44	0.981		34.34	0.974	
45.59	0.99		43.28	0.983		32.51	0.979	
44.00	0.995		41.21	0.988		30.67	0.983	
42.03	0.998		38.98	0.991		28.51	0.988	
40.66	1	1	36.96	0.993		26.53	0.994	
40.29	1.001		34.99	0.996		24.67	0.999	
38.47	1.004		33.33	0.998		24.50	0.999	
36.60	1.008		33.11	0.999		24.38	1	1
35.96	1.009		32.93	1	1	24.23	1.002	
35.65	1.01		32.54	1.002		23.74	1.006	
34.78	1.012		31.36	1.006		22.59	1.018	0.987
33.06	1.017		28.85	1.018		20.62	1.043	0.965
29.25	1.028		24.79	1.044	0.969	17.58	1.092	0.918
23.85	1.054		19.33	1.096	0.926	12.95	1.216	0.831
17.39	1.109	0.913	12.58	1.233	0.839	8.61	1.47	0.691
10.50	1.255	0.816	7.52	1.514	0.685	5.32	1.981	0.516
5.97	1.556	0.680	4.25	2.083	0.523	3.51	2.749	0.386
3.26	2.164	0.519	2.63	2.938	0.383	2.49	3.775	
1.96	3.078		1.77	4.08				
1.27	4.299							
x_1=0.4044								
298 K			373 K			463 K		
p/MPa	V^{tot}/V^{sat}	V^{liq}/V^{tot}	p/MPa	V^{tot}/V^{sat}	V^{liq}/V^{tot}	p/MPa	V^{tot}/V^{sat}	V^{liq}/V^{tot}
57.42	–	0.979	60.41	0.987		46.74	0.972	
55.56	–	0.978	58.52	0.989		45.09	0.975	
53.80	–	0.976	56.48	0.991		43.10	0.979	
51.82	–	0.972	54.49	0.993		41.16	0.984	
49.92	–	0.967	52.59	0.995		39.12	0.989	
46.33	–	0.966	50.83	0.998		37.15	0.994	
41.67	–	0.955	50.59	1	1	35.17	0.999	
34.44	–	0.937	48.30	1.004	–	35.04	1	1
25.37	–	0.896	44.36	1.015	–	34.12	1.006	–
15.38	–	0.804	38.34	1.038	0.966	32.47	1.017	–
8.78	–	0.672	29.81	1.086	0.927	29.78	1.04	0.963
4.80	–	0.505	19.13	1.216	0.826	25.48	1.087	0.919
2.89	–	0.378	11.30	1.487	0.678	18.83	1.206	0.820
			6.33	2.039	0.519	12.51	1.449	0.682
			3.89	2.871	0.374	7.66	1.942	0.507
			2.61	3.983		4.99	2.684	0.376
						3.49	3.676	

[a] Standard temperature uncertainty $u(T)$: 0.02 K; Standard pressure uncertainty $u(p)$: 0.06 MPa; Maximum standard liquid fraction uncertainty u(Liquid fraction percentage): 2.1 %; Maximum standard relative volume uncertainty u(Relative volume): 0.035.

Table 14
Relative volume (V^{tot}/V^{sat}) and liquid fraction (V^{liq}/V^{tot}) for the pseudo-binary system CO_2 (1) + STO (2)[a].

x_1=0.2082								
298 K			373 K			463 K		
p/MPa	V^{tot}/V^{sat}	V^{liq}/V^{tot}	p/MPa	V^{tot}/V^{sat}	V^{liq}/V^{tot}	p/MPa	V^{tot}/V^{sat}	V^{liq}/V^{tot}
15.76	0.948		16.31	0.943		15.63	0.954	
13.67	0.952		16.28	0.946		13.69	0.962	
11.81	0.954		13.75	0.954		11.74	0.967	
9.84	0.956		11.80	0.957		9.72	0.973	
7.87	0.957		9.83	0.961		7.73	0.98	
5.86	0.96		7.58	0.965		5.76	0.988	
4.04	0.963		5.68	0.975		5.51	0.991	
1.96	0.974		3.69	0.98		5.48	0.996	
1.99	0.977		3.64	0.981		5.45	1	1
1.97	0.983		3.64	0.984		5.40	1.009	–
1.94	0.998		3.61	0.989		5.23	1.034	0.973
1.93	1	1	3.57	1	1	4.92	1.086	0.936
1.87	1.027	0.977	3.55	1.003	0.991	4.32	1.214	0.845
1.76	1.087	0.944	3.43	1.031	0.973	3.52	1.47	0.708
1.58	1.237	0.843	3.22	1.087	0.933	2.65	1.983	0.532
1.34	1.536	0.693	2.83	1.226	0.844	2.01	2.754	0.389
1.04	2.134	0.527	2.30	1.506	0.695	1.56	3.782	
0.79	3.032	0.383	1.70	2.065	0.531			
0.61	4.229		1.25	2.905	0.388			
			0.95	4.025				
x_1=0.4000								
298 K			373 K			463 K		
p/MPa	V^{tot}/V^{sat}	V^{liq}/V^{tot}	p/MPa	V^{tot}/V^{sat}	V^{liq}/V^{tot}	p/MPa	V^{tot}/V^{sat}	V^{liq}/V^{tot}
16.72	0.967		18.33	0.972		22.31	0.952	
16.21	0.969		17.90	0.974		21.48	0.958	
14.13	0.976		15.82	0.981		19.53	0.964	
12.13	0.978		13.87	0.984		17.56	0.971	
10.21	0.98		11.84	0.988		15.46	0.978	
8.09	0.983		9.90	0.992		13.50	0.986	
6.25	0.989		7.88	0.997		11.53	0.995	
4.12	0.997		7.74	1	1	11.29	0.999	
3.92	1	1	7.71	1.005	0.997	11.24	1	1
3.90	1.006	0.997	7.59	1.018	0.989	11.23	1.003	–
3.84	1.02	0.991	7.34	1.044	0.972	11.04	1.015	–
3.73	1.048	0.976	6.92	1.097	0.934	10.70	1.038	0.966
3.57	1.105	0.940	6.11	1.229	0.836	10.07	1.085	0.928
3.27	1.247	0.846	5.01	1.493	0.688	8.85	1.202	0.833
2.85	1.531	0.700	3.74	2.023	0.525	7.17	1.438	0.689
2.29	2.099	0.531	2.74	2.818		5.31	1.909	0.522
1.78	2.952	0.392	2.05	3.878		3.90	2.617	0.376
1.37	4.09					2.94	3.562	
x_1=0.6024								
298 K			373 K			463 K		
p/MPa	V^{tot}/V^{sat}	V^{liq}/V^{tot}	p/MPa	V^{tot}/V^{sat}	V^{liq}/V^{tot}	p/MPa	V^{tot}/V^{sat}	V^{liq}/V^{tot}
18.41	0.974		24.37	0.969		31.24	0.937	
18.08	0.976		23.58	0.973		29.10	0.946	
15.89	0.982		21.93	0.977		27.35	0.953	
13.91	0.985		19.97	0.981		25.36	0.962	
12.05	0.987		17.93	0.986		23.41	0.971	
10.09	0.99		15.85	0.992		21.40	0.983	
8.12	0.993		13.89	0.997		19.39	0.996	
6.05	0.998		13.69	0.998		19.28	0.997	
6.06	0.998		13.33	1	1	19.16	1	1
5.79	1	1	13.27	1.004	–	19.09	1.003	–
5.78	1.005	–	13.07	1.016	–	18.81	1.012	–
5.74	1.017	–	12.69	1.038	–	18.29	1.032	–
5.64	1.042	–	12.04	1.083	0.914	17.35	1.071	0.885
5.48	1.092	0.934	10.79	1.196	0.813	15.45	1.169	0.787
5.17	1.216	0.844	9.07	1.422	0.673	12.83	1.365	0.644
4.72	1.465	0.690	7.01	1.875	0.507	9.74	1.758	0.483
4.07	1.963	0.524	5.29	2.556		7.26	2.349	
3.34	2.709		4.02	3.464		5.48	3.139	
2.67	3.705							
x_1=0.7013								
298 K			373 K			463 K		
p/MPa	V^{tot}/V^{sat}	V^{liq}/V^{tot}	p/MPa	V^{tot}/V^{sat}	V^{liq}/V^{tot}	p/MPa	V^{tot}/V^{sat}	V^{liq}/V^{tot}
21.45	0.957		28.50	0.951		29.30	0.916	

(*continued on next page*)

Table 14 (*continued*)

x_1=0.7013								
298 K			373 K			463 K		
p/MPa	V^{tot}/V^{sat}	V^{liq}/V^{tot}	p/MPa	V^{tot}/V^{sat}	V^{liq}/V^{tot}	p/MPa	V^{tot}/V^{sat}	V^{liq}/V^{tot}
20.62	0.962		26.75	0.956		28.52	0.92	
18.73	0.966		24.74	0.961		26.71	0.932	
16.75	0.969		22.76	0.966		24.72	0.948	
14.80	0.972		20.79	0.973		22.67	0.986	
12.80	0.976		18.73	0.98		22.63	0.987	
10.79	0.979		16.87	0.989		22.58	0.989	
8.66	0.984		16.84	0.99		22.47	0.992	
6.68	0.988		16.82	0.992		22.21	1	1
6.49	0.991		16.70	0.996		21.73	1.016	–
6.48	0.996		16.56	1	1	20.82	1.047	–
6.47	1	1	16.42	1.005	–	19.80	1.086	0.720
6.44	1.007	–	15.96	1.024	–	19.30	1.108	0.692
6.37	1.028	–	15.17	1.063	–	18.29	1.158	0.649
6.25	1.072	0.927	13.70	1.16	0.782	17.29	1.213	0.599
6.01	1.18	0.840	11.75	1.355	0.644	16.28	1.278	0.556
5.65	1.398	0.698	10.39	1.549	0.555	15.29	1.352	0.523
5.36	1.615	0.531	8.54	1.94				
4.84	2.05		7.27	2.33				
4.39	2.484							

[a] Standard temperature uncertainty $u(T)$: 0.02 K; Standard pressure uncertainty $u(p)$: 0.06 MPa; Maximum standard liquid fraction uncertainty u(Liquid fraction percentage): 2.1 %; Maximum standard relative volume uncertainty u(Relative volume): 0.035.

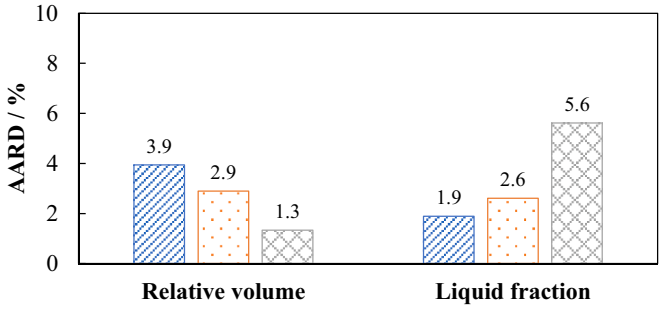

Fig. 20. AARD (%)in the relative volume and the liquid fraction of the N_2 (1) + STO (2) system calculated by SRK (diagonal striped), PR (dotted), PC-SAFT (crosshatched).

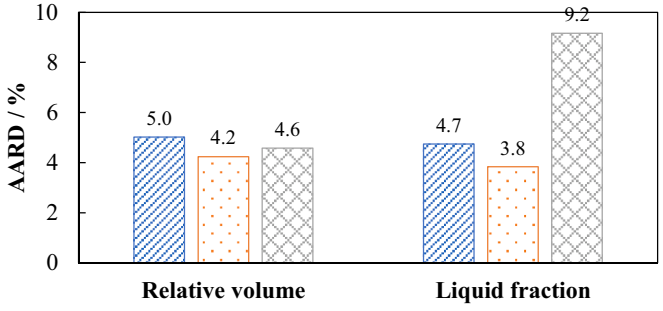

Fig. 21. AARD (%)in the relative volume and the liquid fraction of the CO_2 (1) + STO (2) system calculated by SRK (diagonal striped), PR (dotted), PC-SAFT (crosshatched).

model results in Figs. S3 to S6. The modeling results are highly influenced by the calculated saturation pressures, e.g., the high deviation in p^{sat} for PC-SAFT for CO_2+STO at x_1=0.7013 results in a high deviation in the liquid fraction at the same composition. In general, all the three models can describe the relative volume well and capture the shape of the liquid fraction reasonably well. The AARD% for both systems are given in Figs. 20 and 21. For the relative volume, all the models perform similarly for CO_2+STO, with a deviation around 5%, while PC-SAFT performs much better than the other two for N_2+STO, with a deviation of only 1.3%. For the liquid fraction, PC-SAFT is clearly worse than SRK and PR, with its deviation twice as large.

4. Conclusions

We extended our previous study of CH_4+STO to two other highly asymmetric mixtures: N_2+STO and CO_2+STO. A systematic study of these pseudo-binary mixtures can shed light on the phase behavior of real reservoir fluids, whose ill-defined heavy ends cannot be readily represented by several well-defined components. For both mixtures, we measured their phase equilibrium and densities in the same temperature range from (298.15 to 463.15) K and the same pressure range (up to 140 MPa) as in the previous study [20]. The study provides valuable data for evaluating and improving thermodynamic models for HPHT reservoir fluids and gas injection processes. In this study, we compared SRK, PR, SRK-VT, PR-VT, and PC-SAFT in modeling the measured data.

For density modeling, volume translation is essential to reduce the large deviations of SRK and PR. SRK-VT, PR-VT, and PC-SAFT perform similarly, and SRK-VT gives the smallest deviations for both systems. The good performance of SRK-VT and PR-VT is partly because their C_{7+} volume translation parameters are determined using the C_{7+} densities. The deviations in the live oil density are correlated with those in the STO density, showing the importance of modeling the STO density accurately. For isothermal compressibility modeling, all models give large and comparable deviations.

The deviations in the pseudo-excess molar volumes calculated by SRK, PR, and PC-SAFT are small compared to the corresponding mixture molar volumes. Consequently, it is possible to use the recently proposed excess volume method to estimate the live fluid densities accurately. Using the pseudo-excess molar volumes from any of the three models and the experimental STO densities, the estimated densities have an average deviation of ~0.5% only. This method may significantly reduce the amount of live fluid density measurement.

For saturation pressure prediction, PC-SAFT outperforms SRK and PR for N_2+STO but underperforms for CO_2+STO—this observation seems to be case dependent, e.g., it is different from our previous observation for CH_4+STO. For relative volumes and liquid fractions, these models perform similarly.

With this study and our previous one on CH_4+STO, we have provided high-pressure data for asymmetric mixtures consisting of the same STO and three important light gases (CH_4, N_2, CO_2). Further study may

be considered for systems containing intermediate components or STO with different properties.

CRediT authorship contribution statement

Yiqun Liu: Conceptualization, Data curation, Investigation, Methodology, Validation, Visualization, Writing – original draft. **Teresa Regueira:** Conceptualization, Investigation, Methodology, Project administration, Supervision. **Erling H. Stenby:** Conceptualization, Project administration, Supervision. **Wei Yan:** Conceptualization, Investigation, Methodology, Project administration, Resources, Software, Supervision, Validation, Writing – original draft.

Declaration of Competing Interest

The authors declare that they have no known competing financial interests or personal relationships that could have appeared to influence the work reported in this paper.

Data availability

The authors do not have permission to share data.

References

[1] G. DeBruijn, C. Skeates, R. Greenaway, D. Harrison, M. Parris, S. James, et al., High-pressure, high-temperature technologies, Oilfield Rev. 20 (2008) 46–60.

[2] U.S. Department of the Interior Bureau of Ocean Energy Management. HPHT Production in the Gulf of Mexico, OCS Report BOEM 2020-060. New Orleans, August 2020. https://www.boem.gov/sites/default/files/documents/about-boem/HPHT-Production-in-the-GOM.pdf.

[3] H. Baled, R.M. Enick, Y. Wu, M.A. McHugh, W. Burgess, D. Tapriyal, B.D. Morreale, Prediction of hydrocarbon densities at extreme conditions using volume-translated SRK and PR equations of state fit to high temperature, high pressure PVT data, Fluid Phase Equilib. 317 (2012) 65–76, https://doi.org/10.1016/j.fluid.2011.12.027.

[4] W.A. Burgess, B.A. Bamgbade, I.K. Gamwo, Experimental and predictive PC-SAFT modeling results for density and isothermal compressibility for two crude oil samples at elevated temperatures and pressures, Fuel 218 (2018) 385–395, https://doi.org/10.1016/j.fuel.2017.12.101.

[5] J.F. Estela-Uribe, An improved Helmholtz energy model for non-polar fluids and their mixtures. Part 2: application to mixtures of non-polar fluids, Fluid Phase Equilib. 354 (2013) 326–343, https://doi.org/10.1016/j.fluid.2013.05.004.

[6] J.F. Estela-Uribe, An improved Helmholtz energy model for non-polar fluids and their mixtures. Part 3: application to natural gases and related systems, Fluid Phase Equilib. 356 (2013) 229–345, https://doi.org/10.1016/j.fluid.2013.07.043.

[7] A.Gonzalez Perez, C. Coquelet, P. Paricaud, A. Chapoy, Comparative study of vapour-liquid equilibrium and density modelling of mixtures related to carbon capture and storage with SRK, PR, PC-SAFT and SAFT-VR Mie equations of state for industrial uses, Fluid Phase Equilib. 427 (2016) 371–383, https://doi.org/10.1016/j.fluid.2016.08.002.

[8] W. Yan, T. Regueira, Y. Liu, E.H. Stenby, Density modeling of high-pressure mixtures using cubic and non-cubic EoS and an excess volume method, Fluid Phase Equilib. 532 (2021), 112884, https://doi.org/10.1016/j.fluid.2020.112884.

[9] B. Tohidi, A.C. Todd, A. Danesh, R.W. Burgess, F. Gozalpour, Viscosity and density of methane+cis-decalin from 323 to 424 K at pressures to 140 MPa, Int. J. Thermophys. 22 (2001) 1661–1668, https://doi.org/10.1023/A:1013130731336.

[10] F. Gozalpour, A. Danesh, A.C. Todd, B. Tohidi, Viscosity and density data for a six-component model fluid at temperatures to 423 K and pressures to 140 MPa, High Temp. High Press. 34 (2002) 483–486, https://doi.org/10.1068/htjr041.

[11] F. Gozalpour, A. Danesh, A.C. Todd, D.H. Tehrani, B. Tohidi, Vapour-liquid equilibrium volume and density measurements of a five-component gas condensate at 278.15-383.15 K, Fluid Phase Equilib. 206 (2003) 95–104, https://doi.org/10.1016/S0378-3812(02)00305-9.

[12] F. Gozalpour, A. Danesh, A.C. Todd, B. Tohidi, Experimental data on binary and ternary mixtures of perfluoromethylcyclohexane with methane and n-decane at 373.15 K, J. Chem. Eng. Data 50 (2005) 1814–1817, https://doi.org/10.1021/je049550t.

[13] B.A. Bamgbade, Y. Wu, W.A. Burgess, D. Tapriyal, I.K. Gamwo, H.O. Baled, R. M. Enick, M.A. McHugh, Measurements and modeling of high-temperature, high-pressure density for binary mixtures of propane with n-decane and propane with n-eicosane, J. Chem. Thermodyn. 84 (2015) 108–117, https://doi.org/10.1016/j.jct.2014.12.015.

[14] B.A. Bamgbade, Y. Wu, W.A. Burgess, D. Tapriyal, I.K. Gamwo, H.O. Baled, R. M. Enick, M.A. McHugh, High-temperature, high-pressure volumetric properties of propane, squalane, and their mixtures: measurement and PC-SAFT modeling, Ind. Eng. Chem. Res. 54 (2015) 6804–6811, https://doi.org/10.1021/acs.iecr.5b01173.

[15] T. Regueira, W. Yan, E.H. Stenby, Densities of the binary systems n-hexane + n-decane and n-hexane + n-hexadecane up to 60 MPa and 463 K, J. Chem. Eng. Data 60 (2015) 3631–3645, https://doi.org/10.1021/acs.jced.5b00613.

[16] T. Regueira, G. Pantelide, W. Yan, E.H. Stenby, Density and phase equilibrium of the binary system methane + n-decane under high temperatures and pressures, Fluid Phase Equilib. 428 (2016) 48–61, https://doi.org/10.1016/j.fluid.2016.08.004.

[17] T. Regueira, Y. Liu, A.A. Wibowo, M. Ashrafi, F. Varzandeh, G. Pantelide, E. H. Stenby, W. Yan, High pressure phase equilibrium of ternary and multicomponent alkane mixtures in the temperature range from (283 to 473) K, Fluid Phase Equilib. 449 (2017) 186–196, https://doi.org/10.1016/j.fluid.2017.06.021.

[18] T. Regueira, M.L. Glykioti, E.H. Stenby, W. Yan, Density and compressibility of multicomponent n-alkane mixtures up to 463 K and 140 MPa, J. Chem. Eng. Data 63 (2018) 1072–1080, https://doi.org/10.1021/acs.jced.7b00803.

[19] T. Regueira, M.L. Glykioti, N. Kottaki, E.H. Stenby, W. Yan, Density, compressibility and phase equilibrium of high pressure-high temperature reservoir fluids up to 473 K and 140 MPa, J. Supercrit. Fluids 159 (2020), 104781, https://doi.org/10.1016/j.supflu.2020.104781.

[20] Y. Liu, T. Regueira, E.H. Stenby, W. Yan, High-pressure phase equilibrium and volumetric properties of pseudo-binary mixtures of stock tank oil + methane up to 463 K, Fluid Phase Equilib. 541 (2021), 113054, https://doi.org/10.1016/j.fluid.2021.113054.

[21] G. Soave, Equilibrium constants from a modified Redlich-Kwong equation of state, Chem. Eng. Sci. 27 (1972) 1197–1203, https://doi.org/10.1016/0009-2509(72)80096-4.

[22] D.Y. Peng, D.B. Robinson, A new two-constant equation of state, Ind. Eng. Chem. Fundam. 15 (1976) 59–64, https://doi.org/10.1021/i160057a011.

[23] J. Gross, G. Sadowski, Perturbed-Chain SAFT: An equation of state based on a perturbation theory for chain molecules, Ind. Eng. Chem. Res. 40 (2001) 1244–1260, https://doi.org/10.1021/ie0003887.

[24] B. Lagourette, C. Boned, H. Saint-Guirons, P. Xans, H. Zhou, Densimeter calibration method versus temperature and pressure, Meas. Sci. Technol. 3 (1992) 699–703, https://doi.org/10.1088/0957-0233/3/8/002.

[25] M.J.P. Comuñas, J.P. Bazile, A. Baylaucq, C. Boned, Density of diethyl adipate using a new vibrating tube densimeter from (293.15 to 403.15) K and up to 140 MPa. Calibration and measurements, J. Chem. Eng. Data 53 (2008) 986–994, https://doi.org/10.1021/je700737c.

[26] E.W. Lemmon, R. Span, Short fundamental equations of state for 20 industrial fluids, J. Chem. Eng. Data 51 (2006) 785–850, https://doi.org/10.1021/je050186n.

[27] I. Cibulka, L. Hnědkovský, Liquid densities at elevated pressures of n-alkanes from C5 to C16: a critical evaluation of experimental data, J. Chem. Eng. Data 41 (1996) 657–668, https://doi.org/10.1021/je960058m.

[28] J. Dymond, R. Malhotra, The Tait equation: 100 years on, Int. J. Thermophys. 9 (1988) 941–951, https://doi.org/10.1007/BF01133262.

[29] G. Tammann, The dependence of the volume of solutions on pressure, Z. Phys. Chem. Stoechiom. Verwandtschafts. 17 (1895) 620–636, https://doi.org/10.1515/zpch-1895-1738.

[30] W. Yan, F. Varzandeh, E.H. Stenby, PVT modeling of reservoir fluids using PC-SAFT EoS and Soave-BWR EoS, Fluid Phase Equilib. 386 (2015) 96–124, https://doi.org/10.1016/j.fluid.2014.11.022.

[31] A. Péneloux, E. Rauzy, R. Fréze, A consistent correction for Redlich-Kwong-Soave volumes, Fluid Phase Equilib. 8 (1982) 7–23, https://doi.org/10.1016/0378-3812(82)80002-2.

[32] K.S. Pedersen, P.L. Christensen, Phase Behavior of Petroleum Reservoir Fluids, Taylor & Francis Group, New York, 2007.

[33] T. Yamada, R.D. Gunn, Saturated liquid molar volumes. Rackett equation, J. Chem. Eng. Data 18 (1973) 234–236, https://doi.org/10.1021/je60057a006.

[34] N. von Solms, M.L. Michelsen, G.M. Kontogeorgis, Computational and physical performance of a modified PC-SAFT Equation of State for highly asymmetric and associating mixtures, Ind. Eng. Chem. Res. 42 (2003) 1098–1105, https://doi.org/10.1021/ie020753p.

[35] K.S. Pedersen, A. Fredenslund, P. Thomassen, Properties of oils and natural gases, Gulf Publishing Inc, Houston, 1989.

[36] K.S. Pedersen, P. Thomassen, A. Fredenslund, Characterization of gas condensate mixtures, L.G. Chorn, G.A. Mansoori. Advances in Thermodynamics, Vol.1-C7+ Fraction Characterization, Taylor & Francis, New York, 1989, pp. 137–152.

[37] C.H. Twu, An internally consistent correlation for predicting the critical properties and molecular weights of petroleum and coal-tar liquids, Fluid Phase Equilib. 16 (1984) 137–150, https://doi.org/10.1016/0378-3812(84)85027-X.

[38] G. Soave, Estimation of the critical constants of heavy hydrocarbons for their treatment by the Soave-Redlich-Kwong equation of state, Fluid Phase Equilib. 143 (1998) 29–39, https://doi.org/10.1016/S0378-3812(97)00307-5.

[39] B.I. Lee, M.G. Kesler, A generalized thermodynamic correlation based on three-parameter corresponding states, AIChE J. 21 (1975) 510–527, https://doi.org/10.1002/aic.690210313.

[40] M.G. Kesler, B.I. Lee, Improve prediction of enthalpy of fractions, Hydrocarb. Process. 55 (1976) 153–158.